Chapter 3

Mechanistic and Spectroscopic study for adsorption of Cd^{+2}, Zn^{+2}, Cu^{+2} and Hg^{+2} onto the adsorbents prepared from Palm Shell Powder

Outline:

3.1. Introduction

The utilization of agro waste based adsorbents for the removal of Cu, Cd, Zn and Hg from industrial waste waters and polluted waters has been already recognized (Chapter 1). The biomass has to satisfy the following requirements to be considered as an adsorbent [1]: (1) the efficient and rapid uptake and release of metals, (2) the low production cost of the biosorbent and possibility of its reutilization, (3) the efficient, rapid, and cheap separation of the biosorbent from the solution, and (4) a high selectivity of metal adsorption and desorption. If they are fulfilled, the utilization of the material under study would make the adsorbent more attractive compared to other available adsorbents.

Agricultural by-products usually are composed of lignin and cellulose as major constituents and may also include other polar functional groups of lignin, which includes alcohols, aldehydes, ketones, carboxylic, phenolic and ether groups. These groups have the ability to bind heavy metals by the replacement of hydrogen ions for metal ions in solution or by donation of an electron pair from these groups to form complexes with the metal ions in solution.

Spectroscopic techniques have been a valuable aid in determining functional groups that are responsible for metal binding to *adsorbents.* FT-IR and XPS provide good insight into adsorption process at the molecular level as reported in the literature [2-5]. They have been adopted to identify the major functional groups of adsorbents and elucidate their interactions with metal ions. Both techniques, however, cannot provide a quantitative description of the sorption process, which is important in the design and engineering of treatment systems. Nonetheless, they are essential to provide evidence to further support the formation of mathematical models [6].

Although a considerable amount of research has been carried out on the adsorption of a range of metals by many materials, studies that have focused upon most of the toxic metals using a single adsorbent are rare. Despite the extensive range of materials that have been shown to exhibit adsorptive ability for a range of sorbates, there is still comparatively little understanding of the mechanisms of adsorption. Previous studies have revealed that biosorption of metals is a complex process that is based upon a range of mechanisms that differ both quantitatively and qualitatively according to the type of biosorbent, the degree of processing it has undergone, and also the targeted metal ion. These different mechanisms can include ion exchange, chelation,

adsorption by physical forces, and intraparticle diffusion [7]. A different retention mechanism investigated recently is the amalgamation of Hg(II) on mossy tin filters [8].

Proper analysis and design of adsorption/biosorption separation processes requires relevant adsorption/ biosorption equilibria as one of the vital information. In equilibrium, a certain relationship prevails between solute concentration in solution and adsorbed state (i.e., the amount of solute adsorbed per unit mass of adsorbent). Their equilibrium concentrations are a function of temperature. Therefore, the adsorption equilibrium relationship at a given temperature is referred as adsorption isotherm. Several adsorption isotherms originally used for gas phase adsorption are available and readily adopted to correlate adsorption equilibria in heavy metals biosorption. Some well-known two parameter models are summarized in Table 3.1. Predicting the rate at which adsorption takes place for a given system is probably the most important factor in adsorption system design, with adsorbate residence time and the reactor dimensions controlled by the system's kinetics. A number of adsorption processes for pollutants have been studied in an attempt to find a suitable explanation for the mechanisms and kinetics for sorting out environment solutions. In order to investigate the mechanisms of adsorption, various kinetic models have been suggested. In recent years, adsorption mechanisms involving kinetics-based models have been reported [9]. Numerous kinetic models have described the reaction order of adsorption systems based on solution concentration.

Table 3.1. Common isotherm and kinetics models

Model	Assumptions/comments	Ref.
ISOTHERMS		
Two parameter models		
Langmuir $\frac{q_e}{q_m} = \frac{K_L C_e}{1 + K_L C_e}$	The Langmuir theory is valid for monolayer adsorption onto a surface containing a finite number of identical sites. Langmuir model for isotherm modeling were unsuccessful in the low concentration. Q_m and K_L represent maximum adsorption capacity and energy of adsorption; $0<R_L$ (separation factor)<1 implies favorable adsorption; R_L values indicate the type of isotherm to be irreversible ($R_L = 0$), favorable ($0 < R_L < 1$), linear ($R_L = 1$) or unfavorable ($R_L > 1$). Represents boundary layer diffusion of solute molecules; Uniform energies of adsorption onto the surface and no transmigration of the adsorbate in the plane of the surface. Based on the film resistance and homogeneous solid phase. Two site Langmuir - Presence of two different types of sites (hydrophobic and hydrophillic) on adsorbent favors the applicability of two site model.	[15, 16]

Freundlich $q_e = K_f C_e^{1/n}$	High values for K_f shows high adsorption capacity; Heterogeneous adsorbent and multilayer adsorption and the adsorption capacity is related to the concentration of adsorbate at equilibrium. The constant n is the empirical parameter related to the intensity of adsorption, which varies with the heterogeneity of the material. To describe heterogeneous systems 1/n values indicate the type of isotherm to be irreversible (1/n = 0), favorable (0 < 1/n < 1) and unfavorable (1/n>1) shows the adsorption capacity of an adsorbent, The adsorption process occurs on the heterogeneous surfaces. If the n is below one, then the adsorption is chemical process; otherwise, the adsorption is physical process.	[17]
Temkin $\frac{q_e}{q_m} = \frac{R_T}{\Delta Q}\mathrm{Ln}(K_T C_e)$	Parameters from Temkin model describes The heat of adsorption of all the molecules in the layer decreases linearly with coverage due to adsorbent–adsorbate interactions, and that the adsorption is characterized by a uniform distribution of binding energies, up to some maximum binding energy; K_T equilibrium constant corresponds to maximum binding energy and B1 is related to heat of adsorption.	[18]
Flory Huggins $\mathrm{Log}\frac{\theta}{C_0} = \mathrm{Log}K_{FH} + n_{FH}\mathrm{Log}(1-\theta)$	Account for the degree of surface coverage characteristics of the sorbate on the sorbent.	[19-21]
Elovich $\frac{q_e}{q_m} = K_E C_e exp^{-\left(\frac{q_e}{q_m}\right)}$	The Elovich model is based on a kinetic development according to the hypothesis that the adsorption sites increase exponentially with adsorption, involving multi-layered adsorption.	[22]
Dubinin-Radushkevich $\frac{q_e}{q_m} = \exp(-\beta\varepsilon^2)$ With $\beta = \frac{1}{E^2}$ and $\varepsilon = RT\mathrm{Ln}\frac{C_s}{C_e}$	Dubinin and his co-workers conceived this equation for subcritical vapors in micropore solids where the adsorption process follows a pore filling mechanism onto energetically non-uniform surface.	[23]
Halsey $q_e = K_H/C_e^{1/n_H}$	Halsey proposed an expression for condensation of a multilayer at a relatively large distance from the surface.	[24]
KINETICS		
Pseudo 1st order $\frac{dq}{dt} = K_i'(q_e - q_t)$	Generally do not fit well in whole range of contact time, only follows in initial stage of sorption. The adsorbate uptake, q, increases with increasing the initial concentration.	[25]
Pseudo 2nd order $q_t = \frac{q_e^2 K_2' t}{1 + q_e K t}$	The adsorption rate of adsorbate depends on the concentration of adsorbate at the absorbent surface. Mechanism being the rate controlling step, involve valency forces through sharing or exchange of electrons between adsorbate and adsorbent. Kinetic performance is proportional to the adsorption rate. Based on the sorption equilibrium capacity. The adsorption process and the overall rate of the adsorption process appears to be controlled by the chemical reaction. Chemisorption significantly contribute to the adsorption process	[26]
Intraparticle $q_t = K_i t^{0.5}$	Commonly used to identify the steps involved in adsorption. If it passes through origin it infers the applicability of intraparticle diffusion whereas presence of intercept shows the surface adsorption/ boundary layer effects. Adsorption is said to be intra-particle diffusion controlled if the reaction sites are internally located in the porous adsorbents and the external resistance to diffusive transport process is much less than the internal resistance. The term k_{dif} calculated from the slope is indicative of an enhancement in the rate of adsorption. The value of C from intercept gives an idea about the boundary layer thickness. Adsorption is said to be intra-particle diffusion controlled if the reaction sites are internally located in the porous adsorbents and the external resistance to diffusive transport process is much less than the internal resistance.	[27-29]

Elovich model $q_t = \frac{1}{\beta}\mathrm{Ln}(\alpha\beta) + \frac{1}{\beta}\mathrm{Lnt}$	Considers that the rate-controlling step is the diffusion of the adsorbate molecules. The Elovich equation describes chemisorption.	[30-32]
Liquid film diffusion model $\frac{q_t}{q_e} = 1 - \frac{6}{\pi^2}\exp(-\mathrm{Bt})$ $\mathrm{Ln}(1-\mathrm{F}) = -\mathrm{K_{fd}t}$	Determines whether the main resistance to mass transfer is in the thin film (boundary layer) surrounding the adsorbent particle, or in the resistance to diffusion inside the pores. Applicable when flow of the reaction from the bulk liquid to the surface of the adsorbent determines the rate constant.	[33]
Bangham $\mathrm{LogLog}\left(\frac{C_0}{C_0 - q_t m}\right) = \mathrm{Log}\left(\frac{K_m}{2.303V} + \propto \mathrm{Log}t\right)$	Applicability of the Bangham equation indicates that diffusion of adsorbate into the pores of adsorbent is importantly controls the adsorption process. It is a pore diffusion controlled process.	[34]
Column Models		
Thomas Model $ln\left(\frac{C_0}{C} - 1\right) = \frac{K_T q_0 m}{Q}$	This model assumes plug-flow behaviour in the bed and uses the Langmuir isotherm for equilibrium and second-order reversible reaction kinetics. It assumes a constant separation factor but is applicable to both favorable and unfavorable sorption conditions. This model is suitable for sorption processes in which external and internal diffusion limitations are absent.	[11]
Yoon and Nelson Model $\ln\left(\frac{C}{C_0 - C}\right) = \mathrm{k_{YN}t} - \mathrm{t_{0.5}k_{YN}}$	Relatively simple model based on the assumption that the rate of decrease in the probability of sorption for each sorbate molecule is proportional to the probability of sorbate sorption and sorbate breakthrough on the sorbent.	[12]
Wolborska Model $\ln\frac{C}{C_0} = \frac{\beta C_0}{N_0}\mathrm{t} - \frac{\beta Z}{U}$	Wolborska deduced the following relationship for describing the concentration distribution in a bed for the low-concentration range of the breakthrough curve.	[14]

3.1.1. Column studies.

Batch operations are very easy to apply in the laboratory study, but less convenient for field applications. The sorption capacity of the sorbent, obtained from batch equilibrium experiments, is useful in providing fundamental information about the effectiveness of metal–sorbent system. However, this data may not be practically applicable to most of the treatment systems (such as continuous modes) where contact time is not sufficient for the attainment of equilibrium. Thus, it is necessary to ascertain the practical applicability of the adsorbent in fixed bed column modes. Fixed-bed adsorption is used to determine the experimental breakthrough curve. Several models have been reported for predicting the breakthrough performance in fixed-bed sorption [10-14].

3.1.2. Desorption.

Desorption studies are important to investigate the possibility for the recovery of metals adsorbed on the adsorbent surface, as well as for the regeneration of the adsorbent for subsequent reuse. It also gives a hint about the mechanism of ineraction between the adsorbent and adsorbate. For instance, if acid medium employed for recovery, protons appear to compete with the metal ions and displace them from the adsorbent's surface, suggesting that adsorption of metal ions involve mainly ion-exchange mechanisms. On the other hand if a complexing agent like EDTA is effective, it suggests a complexation mechanism of interaction between adsorbent and adsorbate. The main objective will be:

i) To investigate the copper, cadmium, zinc and mercury removal efficiency and adsorption capacity of the adsorbents which had been prepared and characterized as described in chapter 2 (PSP, APSP, SAPSP, PAPSP, 9AAC and MPSP).

ii) To study the effects of adsorbent dosage, pH, contact time, adsorbate concentration, and solution temperature.

iii) To determine and discuss the thermodynamic parameters and kinetic data, equilibrium isotherms by using the models described in Table 3.1.

iv) To obtain structural as well as analytical information about the metal biomass interactions, through Fourier transform infrared (FTIR) and the X-ray photoelectron (XPS) spectroscopic techniques

v) To perform desorption experiments to determine the feasibility of reusing the adsorbents under study vi) study the performance of the adsorbents in flow through columns experiments

3.2. Materials and Methods

3.2.1. Batch Uptake.

Stock solutions of Cu^{2+}, Cd^{2+}, Zn^{2+} and Hg^{2+} was prepared by dissolving 3.84, 2.77, 4.59 and 1.36 g of copper nitrate, cadmium nitrate, zinc nitrate and mercuric chloride (E-Merck) in slightly acidified double distilled water and making upto 1L to give 1000 mg/L of Cu^{2+}, Cd^{2+}, Zn^{2+} and Hg^{2+} solutions respectively. Working standards were prepared by diluting different volumes of the stock solution to obtain the desired concentration.

Batch adsorption experiments were conducted at 30°C by agitating 0.1 g of adsorbent with 25mL of respective metal ion solution of desired concentration maintained at pH 6.0 (except for pH experiments) in 100mL stoppered conical flasks in a thermostated rotary mechanical shaker at 180 rpm for 4 hours (except for the contact time experiments) at 30 °C. Experiments were done to determine the pH range at which the maximum metal uptake would take place on the adsorbents under study by varying the initial pH of the solution in the range 1 to 10 (except copper i.e. pH 1-5) using 0.1 N NaOH and/or HCl. The effect of the initial concentration (1 to 1000 mg/L) was also studied in order to determine the effect of the parameter on the adsorption of metal from the solution. The optimum equilibrium time was determined as the contact time required for the concentration of metal in the solution to reach equilibrium and was obtained by varying the contact time in the range 30 to 240 minutes.

At the end of the predetermined time intervals, the suspensions were filtered and the Cu^{2+}, Cd^{2+}, Zn^{2+} and Hg^{2+} content in the filterate was analysed by using AAnalyst 200 Perkin-Elmer atomic absorption spectrophotometer. The uptake of Cu^{2+}, Cd^{2+}, Zn^{2+} and Hg^{2+} by the adsorbents under study (q_e) was calculated from the difference between the initial and final concentration as follows:

$$q_e = (C_i - C_e)/m; \quad (1)$$

Where, C_i-initial concentration of metal ion mg/L; C_e – Equilibrium concentration of metal ion mg/L; m – Mass of adsorbent g/L; q_e – Amount of metal ion adsorbed per gram of adsorbent. Each experimental result was obtained by averaging the data from three parallel experiments.

Adsorption isotherm experiments were also performed by agitating 0.1 g of the adsorbent under study with a series of 25 mL solutions at optimum pH, containing different initial concentrations of (1 to 1000 mg/L) at 30 °C. After the established contact time was attained, the suspension was filtered, and supernatant was analyzed for the metal concentration. The

adherence of the equilibrium isotherm and data obtained to different adsorption isotherms models as given in Table 3.1 was tested.

Similarly the Cu^{2+}, Cd^{2+}, Zn^{2+} and Hg^{2+} adsorption data obtained after agitating solutioncontaining 10 mg/L of Cu^{2+}, Cd^{2+}, Zn^{2+} and $Hg^{2+}$for various contact times with the adsorbents under study at optimum pH obtained and were modeled to determine the order of reaction rate and the adherence to different kinetic models as given in Table 3.1 was tested.

Thermodynamic parameters of the adsorption process (ΔG^0, ΔH^0 and ΔS^0) could be determined from the experimental data obtained at various temperatures using following equations:

$$ln\frac{q_e}{C_e} = \frac{\Delta S^0}{R} - \frac{\Delta H^0}{RT} (2)$$

$$\Delta G^0 = \Delta H^0 - T\Delta S^0 (3)$$

where R is the gas constant (8.314 $Jmol^{-1}K^{-1}$) and T is the absolute temperature (K). Values of correlation coefficients and standard deviation were used to compare the models. SD was calculated using the equation.

$$SD = \sqrt{\frac{1}{N}\sum_{i=1}^{N}(x_i - \bar{x})^2} (4)$$

3.2.2. Desorption Studies.

0.1 g of metal loaded adsorbents under study was treated with 10 mL of 0.1 M EDTA, 0.1M NH_3 and 0.1M HCl for a period of 60 min in a thermostated rotary mechanical shaker. After 60 min the amount of metal desorbed from the adsorbents under study was determined by AAS. The adsorption-desorption experiments were repeated for three cycles.

3.2.3. Column Studies.

Column experiments were conducted in a glass column with an internal diameter of 1 cm and a length of 30 cm packed with the adsorbent under study. Cu^{2+}, Cd^{2+}, Zn^{2+} and Hg^{2+} solution of known concentration (1000 mg/L) at optimum pH was passed through the column of adsorbent at a flow rate of 1 mL/min. Samples from the column effluent were collected at regular intervals and analyzed by atomic absorption spectrometry. The break-through time has been chosen when the concentration of the effluent is 1 mg/L.

3.2.4. Spectroscopic Analysis.

FT-IR spectra for biosorbent and the metal-loaded biosorbents were obtained using a Perkin Elmer RX1 model within the wave number range of (400 to 4000) cm^{-1}.

The surface of the Cu and Hg–loaded samples was analyzed using a KRATOS AXIS 165 X-ray Photoelectron spectrometer. Peak fitting and presentation output are produced by an integrated VISION control and information system. The deconvolution process of C 1s spectra as well as the elemental composition evaluation may result in an error of up to 5%. All spectra are presented charge balanced and energy referenced to C 1s at 284.6 eV [35].

The ^{13}C-NMR experiments were performed with a Bruker Avance (300 MHz) spectrometer for Cu–loaded samples. The chemical shifts δ, expressed in parts per million [ppm], were referenced relative to the signal of tetramethylsilane (TMS) at $\delta c = 0$ ppm.

3.3. Results and Discussion

3.3.1. Uptake studies.

3.3.1.1. ***pH Dependence***.The pH of the medium from which adsorption is taking place is an important controlling parameter in heavy metal adsorption process. Hence uptake of Cd^{2+}, Zn^{2+} and Hg^{2+} has been studied with respect to pH (1-10) whereas uptake of Cu^{2+} was studied within pH (1-5) as shown in Figure 3.1. pH of the solution remains unchanged after the adsorption experiment.

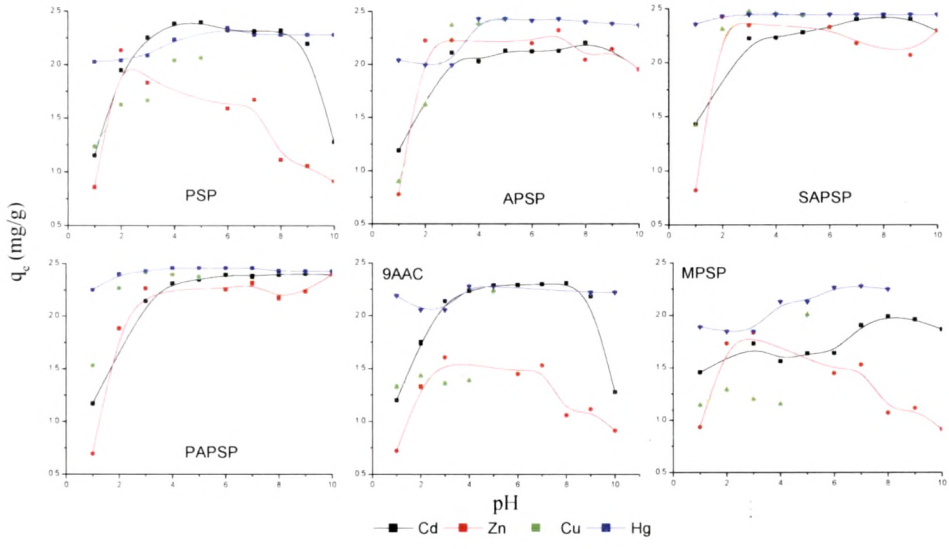

Operating parameters: 180 rpm, 10ppm of M^{2+}, 0.1g adsorbent, time 240 min, temperature 30 ^{0}C

Figure 3.1. Effect of pH on adsorption of metal ions

Cd^{2+} and Zn^{2+}:As all the metal exists as ions at a low pH (<4.0), the sharp increase observed in the adsorption of Cd^{2+} and $Zn^{2+}$from pH 1 to 3(more prominent in the case of PSP, APSP, SAPSP and PAPSP) cannot be attributed to the presence of different forms of metal species [36]. This implies that the functional groups on the adsorbents and their ionized forms under these pH conditions determine the extent of adsorption.

It can be presumed that the mechanism for removal of M^{2+}can be by ion-exchange and electrostatic interaction depending on the solution pH. At pH<pK_a of carboxylic groups, the removal could be due to ion-exchange process, as the binding sites are protonated. However, at

pH >pK_a, the carboxyl groups are negatively charged, the metal ions may bind to the binding sites by electrostatic attraction [41]. The hydroxyl groups can also become negatively charged at high pH, thereby contributing to metal removal at high pH (7 to 10).

Specific interactions of metal ion species with adsorbent surface and/or the existence of preferential adsorption sites may also affect the metal adsorption and could be responsible for the slight differences found in the adsorptive behavior of M^{2+} ions with pH variation [37]. Optimum adsorption above pH 3 has been reported for M^{2+} uptake on some other agro based activated carbons [38, 39].

Cu^{2+}: In case of PSP, APSP, SAPSP and PAPSP adsorption increased with increase in pH till pH 4, 3.5, and 2.9 respectively for Cu^{2+} and then remained constant. Compared to other adsorbents APSP showed a sharp increase in adsorption of copper between pH 1 to 3.5 probably due to the presence of more number of carboxyl groups as evidenced by FT-IR, NMR and XPS. On the other hand, for MPSP and 9AAC adsorption remained constant till pH 3.5 and 4 and then increased giving maximum adsorption at pH 5. The possible reason could be that 9AAC and MPSP had lesser number of carboxyl groups and more of phenolic groups and metal ions mainly exchanged with –COOH groups of natural biomass between pH 1.5 and 5, while at higher pH, phenol groups might become more active Cu^{2+} sorption sites. Above pH_{Zpc} (PSP 3.298; APSP3.719; SAPSP 3.718; PAPSP 4.21; 9AAC 3.085; MPSP 3.155) the surface is negatively charged and hence attracts copper cations.

Hg^{2+}: Figure 3.1 shows that adsorption of mercury reaches maximum at ~pH 3.5 and is constant for the entire range of pH studied for all the adsorbents . This high adsorption is believed to be associated with the formation of positively charged metal hydroxy species having strong affinity for surface functional groups. The observed reduced adsorption at low pH value (2.0) may be attributed to (i) higher hydrated species [Hg^{2+} (aq) species] having low mobility and (ii) protonation of the surface functional groups as well as the competition between mercuric ions and H^+ or H_3O^+ ions present in the solution. At higher pH values (3.0), more functional groups are available for metal ion binding due to deprotonation, resulting in high adsorption. Thereby, maximum adsorption of mercury from pH 3.0 may be due to partial hydrolysis forming $HgCl^+$, $HgClOH^+$, and $Hg(OH)_2$ species, having strong affinity for the negatively charged functional groups of the adsorbents under study.(need to give references which were given in paper)

However adsorption capacity for mercury is still > 90% in acidic pH conditions. This

implies that an acidic group is responsible for mercury binding at low pH, while a weak acidic group such as carboxyl group is dominant at neutral pH *(15)*. The initial rapid uptake of Hg (II) from solution may likely be due to binding of adsorbate ions on the surface of the adsorbents through ion-exchange process. This instantaneous surface adsorption causes a rapid increase in Hg (II) uptake. Later on slower adsorption might be due to intraparticle diffusion, and diffusion of mercury from the aqueous phase to the adsorbents under study.

At pH values above 8.3, 7.1, 4.6 and 8.5; Cd, Zn, Cu and Hg respectively precipitates in the form of metal oxides or hydroxides are formed [40]. It was decided to perform all the adsorption studies at pH of 6 for Cd^{2+}, Zn^{2+}, Hg^{2+}; whereas Cu^{2+} was studied at pH 4.5.

3.3.1.2. ***Contact Time Dependence***. The effect of contact time variation on adsorption of Cd^{2+}, Zn^{2+}, Cu^{2+} and Hg^{2+} was studied and the results are shown in Figure 3.2.

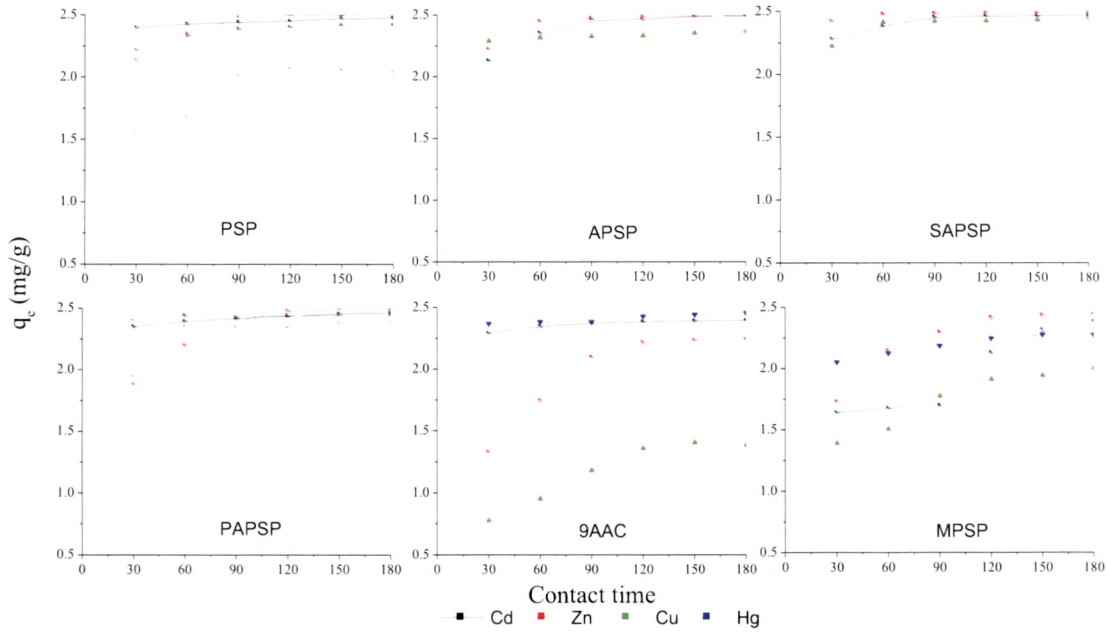

Operating parameters: 180 rpm, 10ppm of M^{2+}, 0.1g adsorbent, temperature 30 ^{0}C, optimum pH

Figure 3.2. Effect of contact time of M^{2+}

It is seen that more than 50% of M^{2+} was adsorbed within 60 min and equilibrium adsorption was attained in 1590 min for all the adsorbents but optimum time for adsorption equilibrium was fixed as 180 min. The rate of adsorption is very fast initially followed by a

decreased rate with the approach of equilibrium. The removal rate is high initially due to the presence of free binding sites which gradually become saturated with time resulting in decreased rate of adsorption as equilibrium approaches. This indicates that the adsorption is mainly through surface binding. Similar observations were made by Das et al [42].

3.3.1.3. *Dosage dependence*. The effect of variation in dose of the adsorbent was studied to obtain the saturation limit of the adsorbent to adsorbate ratio (Figure 3.3).

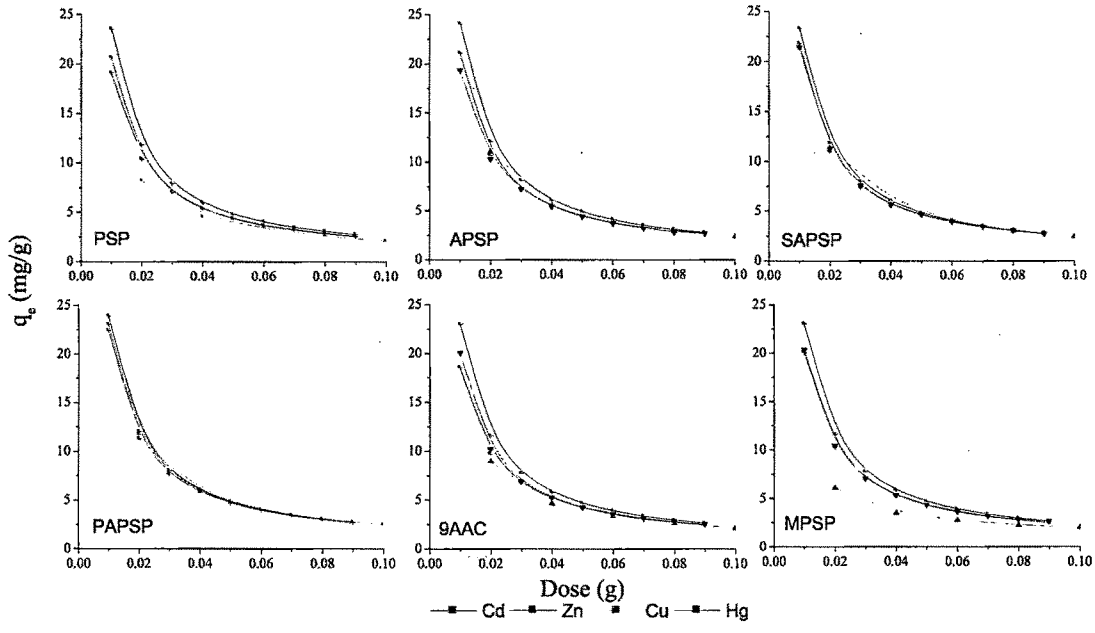

Operating parameters: 180 rpm, time 240 min, temperature 30 ^{0}C, optimum pH

Figure 3.3. Effect of initial concentration of M^{2+}

It was observed that when the adsorbent dose was higher than 0.06 g the metal ion uptake remained almost constant. Increase in the percentage uptake of metal ions with adsorbent dosage could be attributed to increase in the adsorbent surface area and hence the adsorption sites available for adsorption. On the other hand, it is also seen that the increase in the adsorbent dosage leads to a decrease in the q_e. The decrease in q_e value may be due to the concentration gradient between adsorbate and adsorbent with increasing adsorbent concentration causing a decrease in amount of metallic ion adsorbed per gram of adsorbent under study [43].

3.3.1.4. ***Temperature Dependence.*** The effect of temperature variation (Figure 3.4) showed almost same trend for the adsorbents under study. The uptake was found to decrease with increase in temperature indicating that the mechanism of adsorption is exothermic in nature.

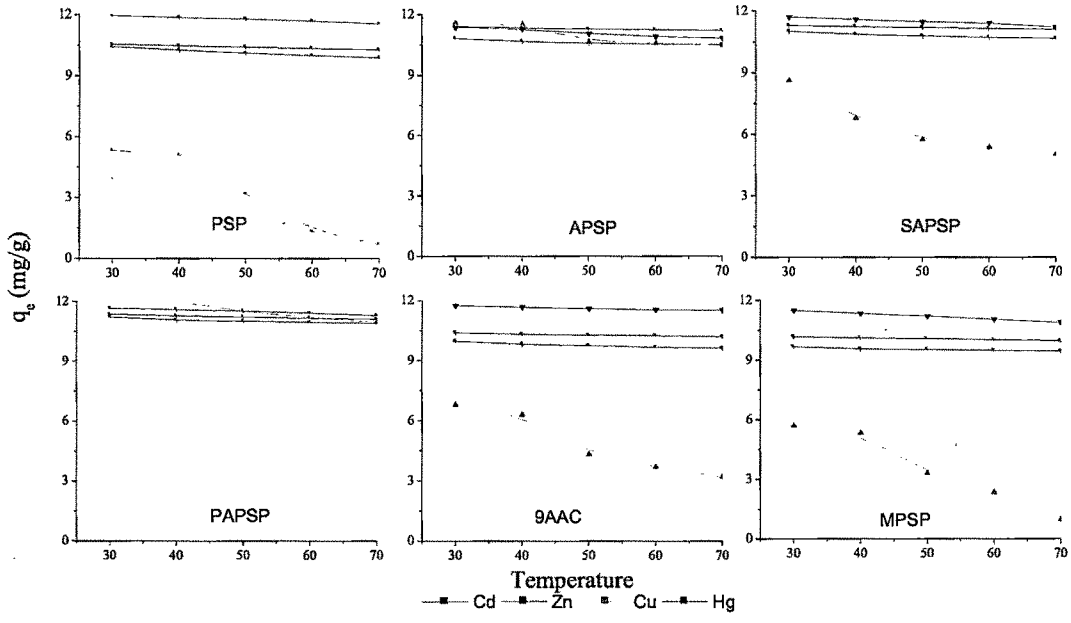

Operating parameters: 180 rpm, 10 ppm of M^{2+}, 0.1g adsorbent, time 240 min, optimum pH

Figure 3.4. Effect of temperature on uptake of M^{2+} ions by PSP, MPSP, APSP, SAPSP, PAPSP and 9AAC

3.3.2. Adsorption Kinetics.

The kinetics of adsorption process describes the solute uptake, which, in turn governs the residence time of the adsorption reaction. The kinetic models of pseudo first order, pseudo second order, intra-particle diffusion, Bangham, Elovich and Liquid film diffusion models were studied. Adsorption kinetics for Cd^{2+}, Zn^{2+}, Cu^{2+} and Hg^{2+} removal by each of the adsorbents under study was conducted at optimum pH and the kinetic constants for the adsorption kinetics are presented in Table 3.2.

Table 3.2. Adsorption kinetic parameters for Cd^{2+}, Zn^{2+}, Cu^{2+} and Hg^{2+} adsorption

Cd^{2+}/ Zn^{2+}						
	PSP	**APSP**	**SAPSP**	**PAPSP**	**9AAC**	**MPSP**
q_e (exp)(mg.g^{-1})	2.573/ 2.591	1.632/ 2.668	2.514/ 2.794	1.594/ 2.804	1.061/ 2.927	2.376/ 2.636
Pseudo 2nd Order						
q_e (mg.g^{-1})	2.492/ 1.605	2.792/ 1.593	2.577/ 2.336	2.501/ 2.448	2.493/ 2.447	1.424/ 2.427
K_2 (g.mgmin^{-1})	0.254/ 0.062	0.009/ 0.060	0.070/ 0.106	0.148/ 0.047	0.174/ 0.049	0.702/ 0.113
r^2	0.999/ 0.997	0.953/ 0.996	0.998/ 0.999	0.999/ 0.999	0.999/ 0.997	1.000/ 0.999
SD	0.056/ 0.088	0.099/ 0.59	0.034/ 0.054	0.022/ 0.066	0.083/ 0.060	0.032/ 0.058
Lagergren						
q_e (mg.g^{-1})	0.219/ 2.453	14.39/ 1.877	6.800/ 1.184	0.718/ 11.26	0.765/ 0.502	0.610/ 1.853
K_1 (min^{-1})	-0.03/ -0.04	-0.05/ -0.04	-0.06/ -0.04	-0.05/ -0.06	-0.04/ -0.03	-0.04/ -0.03
r^2	0.821/ 0.799	0.671/ 0.807	0.855/ 0.858	0.836/ 0.778	0.821/ 0.878	0.901/ 0.684
SD	0.074/ 0.058	0.096/ 0.087	0.079/ 0.027	0.039/ 0.071	0.073/ 0.037	0.069/ 0.033
Intraparticle Diffusion						
K_{ip} (mg.gmin$^{-0.5}$)	0.024/ 0.029	0.018/ 0.029	0.005/ 0.021	0.012/ 0.042	0.030/ 0.020	0.025/ 0.039
r^2	0.917/ 0.938	0.976/ 0.917	0.765/ 0.979	0.948/ 0.934	0.985/ 0.957	0.879/ 0.972
SD	0.034/ 0.025	0.007/ 0.029	0.013/ 0.010	0.013/ 0.041	0.018/ 0.014	0.045/ 0.021
Elovich						
β (g.mg^{-1})	23.13/ 8.00	2.21/ 8.00	4.98/ 10.72	9.437/ 4.674	15.58/ 11.43	18.23/ 5.74
α (mg.g^{-1}min^{-1})	4.478E+50/ 1100001	0.329/ 825703	5641180/ 1.981E+18	2.289E+17/ 137142	9.771E+31/ 9.283E+20	8.388E+36/ 452
r^2	0.983/ 0.882	0.765/ 0.855	0.887/ 0.961	0.892/ 0.949	0.995/ 0.926	0.954/ 0.979
SD	0.004/ 0.034	0.085/ 0.038	0.050/ 0.014	0.027/ 0.036	0.004/ 0.018	0.009/ 0.018
Liquid film diffusion model						
K_{FD}	0.025/ 0.043	0.047/ 0.031	0.063/ 0.056	0.04/ 0.062	0.037/ 0.033	0.049/ 0.027
r^2	0.815/ 0.799	0.671/ 0.659	0.854/ 0.789	0.927/ 0.777	0.821/ 0.684	0.902/ 0.878
SD	0.063/ 0.041	0.065/ 0.033	0.064/ 0.082	0.073/ 0.088	0.090/ 0.089	0.089/ 0.054
Bangham						
K_{BM}	0.569/ 0.218	-0.021/ 0.214	0.376/ 0.455	0.491/ 0.311	0.538/ 0.487	0.126/ 0.149
α	4E-04/ 0.002	0.005/ 0.002	0.002/ 9E-04	0.001/ 0.022	7E-04/ 9E-04	6E-04/ 0.01
r^2	0.984/ 0.882	0.765/ 0.855	0.889/ 0.961	0.900/ 0.949	0.754/ 0.926	0.955/ 0.979
SD	0.001/ 0.001	0.001/ 0.001	0.001/ 0.001	0.001/ 0.001	0.001/ 0.001	0.001/ 0.001
Cu^{2+}/ Hg^{2+}						
q_e (exp) (mg/g)	1.662/ 2.178	1.956/ 2.105	2.332/ 2.482	2.712/ 2.455	2.429/ 2.079	1.615/ 1.923
Pseudo 2nd order						
q_e (mg/g)	1.492/ 2.462	1.560/ 2.448	2.406/ 2.449	2.482/ 2.479	2.455/ 2.346	1.742/ 2.173
k_2(g/mgmin)	0.496/ 0.129	0.001/ 0.783	0.079/ 0.777	0.309/ 0.168	0.158/ 0.079	0.015/ 0.124
r^2	0.993/ 0.999	0.971/ 0.999	0.999/ 0.999	0.999/ 0.999	0.999/ 0.999	0.978/ 0.999
SD	0.054/ 0.115	0.048/ 0.089	0.077/ 0.104	0.023/ 0.061	0.059/ 0.019	0.972/ 0.289
Lagergren						
q_e (mg/g)	0.427/ 0.479	0.733/ 0.106	0.315/ 0.045	0.166/ 0.142	0.384/ 0.503	1.202/ 0.318
k_1(min^{-1})	0.012/ 0.030	0.005/ 0.030	0.012/ 0.045	0.022/ 0.011	0.027/ 0.022	0.007/ 0.022
r^2	0.903/ 0.998	0.827/ 0.991	0.887/ 0.529	0.913/ 0.858	0.941/ 0.971	0.928/ 0.916
SD	0.027/ 0.037	0.088/ 0.028	0.097/ 0.042	0.034/ 0.035	0.033/ 0.011	0.087/ 0.023
Intra Particle Diffusion						
k_i(mg/gmin$^{0.5}$)	0.043/ 0.024	0.000/ 0.005	0.182/ 0.018	0.128/ 0.012	0.056/ 0.030	0.162/ 0.025
r^2	0.996/ 0.918	0.000/ 0.976	0.972/ 0.765	0.991/ 0.949	0.968/ 0.985	0.929/ 0.879
SD	0.008/ 0.034	0.000/ 0.008	0.092/ 0.013	0.040/ 0.013	0.029/ 0.018	0.019/ 0.045
Elovich						
β (g.mg^{-1})	12.55/ 8.92	3.953/ 22.472	6.83/ 44.44	17.09/ 19.53	8.514/ 7.353	3.953/ 8.375
α (mg.g^{-1}min^{-1})	0.969/ 4.153E+15	0.119/ 9.57E+48	0.916/ 8.09E+101	0.606/ 1.938E+41	0.391/ 7.911E+10	0.514/ 8.032E+11

r^2	0.824/ 0.962	0.872/ 0.951	0.949/ 0.819	0.845/ 0.911	0.826/ 0.991	0.872/ 0.930
SD	0.099/ 0.024	0.108/ 0.010	0.037/ 0.012	0.028/ 0.017	0.061/ 0.014	0.108/ 0.035
Liquid film diffusion model						
k_{fd} (min^{-1})	-0.01/ -0.07	0.009/ -0.153	-0.013/ -0.03	-0.022/ -0.04	-0.027/ -0.06	-0.01/ -0.06
r^2	0.903/ 0.919	0.954/ 0.874	0.887/ 0.656	0.913/ 0.814	0.941/ 0.992	0.928/ 0.904
SD	0.092/ 0.076	0.072/ 0.079	0.053/ 0.086	0.038/ 0.099	0.036/ 0.083	0.101/ 0.093
Bangham						
K_{BM} ($mL.g^{-1}.L^{-1}$)	-119/ -130	-115/ -142	-114/ -114	-116/ -135	-123/ -131	-124/ -139
α	0.049/ 0.098	0.019/ 0.182	0.009/ 0.009	0.022/ 0.160	0.063/ 0.132	0.059/ 0.160
r2	0.959/ 0.813	0.953/ 0.937	0.819/ 0.891	0.912/ 0.904	0.992/ 0.938	0.926/ 0.937
SD	0.005/ 0.023	0.002/ 0.022	0.002/ 0.001	0.003/ 0.025	0.003/ 0.016	0.008/ 0.019

APSP, SAPSP and PAPSP showed better kinetics attaining equilibrium in ~60 min. followed by PSP attaining equilibrium in 90 min. 9AAC and MPSP attained equilibrium for all the four metal ions in 120 and 150 min respectively. Adsorption capacity at equilibrium was found to be in following order Cu^{2+}<Cd^{2+}~Zn^{2+}~Hg^{2+}.The pseudo second order kinetics provided the best fit for the kinetic data. The q_e values were very close to the experimental q_e values and correlation coefficient values were ~0.99 for PSP, APSP, SAPSP, PAPSP, 9AAC and MPSP for all the metal ions under study suggesting that the rate limiting step in adsorption of metal is chemisorption involving valence forces through the exchange of electrons between adsorbent and adsorbate, complexation, coordination and/or chelation. In pseudo first order the $q_{e(exp)}$ values were much higher than q_e fitted values suggesting that the reaction cannot be classified as first order although this plot has reasonably good correlation coefficient from the fitting process.

The kinetic constants obtained from the Elovich equation are presented in Table 3.2. The results demonstrate a significant relationship between the metal ion adsorbed, q_t, and in these studies with regression coefficients >0.98 and low standard deviation values. Therefore, the kinetic data of the metal ions for all the adsorbents under study showed satisfactory compliance with the Elovich equation. The Liquid film diffusion model is applicable when flow of the reaction from the bulk liquid to the surface of the adsorbent determines the rate constant. The applicability of the model is found to be good as inferred from the values of r^2. The curves did not pass though origin as required by the model but very small intercepts indicates that diffusion of metal from the liquid phase to the adsorbent surface might be having some role in deciding the rate processes.

The Weber and Morris adsorption kinetic model was plotted using equation given in Table 3.1. The plots obtained for PSP, APSP, SAPSP, PAPSP, 9AAC and MPSP do not pass through origin implying that the intra-particle diffusion is not the only operative mechanism.

Bangham equation was applied to the adsorption data with reasonable correlation coefficients confirming the applicability of Bangham equation, thus indicating that diffusion of metal into the pores of adsorbent correlates the adsorption process. However the not so linear curves indicate that the diffusion of adsorbate into pores of the sorbent is not the only rate controlling step.

The study of the various kinetic models reveals that the rate limiting step is chemisorptions and diffusion of adsorbate from the liquid phase to the adsorbent surface and into the pores of the adsorbent might be having some role in deciding the rate processes.

3.3.3. Adsorption Isotherms.

For modeling of cadmium uptake Freundlich, Langmuir, Temkin, Dubinin-Radushkevich (DR), Flory-Huggins, Elovich and Halsey isotherm models (Table 3.1) were employed. The values of fitted model constants for adsorption of M^{2+} on PSP, APSP, SAPSP, PAPSP, 9AAC and MPSP along with their correlation coefficients, r^2 and SD values for all the system studied are presented in Table 3.3.

Table 3.3. Adsorption isotherm parameters for Cd^{2+}, Zn^{2+}, Cu^{2+} and Hg^{2+}

Cd^{2+}/ Zn^{2+}						
	PSP	**APSP**	**SAPSP**	**PAPSP**	**9AAC**	**MPSP**
q_e (exp) ($mg.g^{-1}$)	226/ 203	233/ 202	230/ 215	232/ 216	223/ 219	217/ 204
Freundlich						
$K_f(mg.g^{-1})(dm^3/mg)^{1/n}$	1.45/ 1.20	1.28/ 1.05	1.98/ 1.23	1.62/ 1.39	1.69/ 1.61	1.13/ 0.882
N	1.08/ 1.06	1.05/ 01.01	1.38/ 1.01	1.15/ 1.08	1.22/ 1.15	0.982/0.911
r^2	0.994/0.999	0.997/0.997	0.995/0.999	0.999/0.999	0.999/0.999	0.994/0.998
SD	0.044/0.038	0.017/0.075	0.044/0.021	0.067/0.019	0.066/0.055	0.043/0.059
Langmuir						
K_L ($dm^3.mg^{-1}$)	0.004/0.009	0.008/0.005	0.006/0.007	0.005/0.008	0.005/0.009	0.005/0.010
q_m ($mg.g^{-1}$)	282/ 204	187/ 230	298/ 228	364/ 238	347/ 193	154/ 243
ΔG ($kJ.mol^{-1}$)	-14.0/-12.2	-12.5/ -13.6	-13.2/ -12.9	-13.9/ -12.6	-13.9/ -11.9	-13.6/ -11.6
r^2	0.961/0.982	0.915/0.999	0.926/0.997	0.890/0.964	0.949/0.990	0.998/0.979
SD	0.063/0.054	0.043/0.002	0.058/0.004	0.065/0.071	0.049/0.003	0.024/0.097
Temkin						
$-\Delta H$ ($kJ.mol^{-1}$)	14.91/11.62	8.90/ 11.79	17.13/13.51	20.87/14.24	21.77/12.08	8.49/7.82
K_T ($dm^3.mg^{-1}$)	0.146/0.126	0.118/0.100	0.227/0.162	0.214/0.178	0.222/0.198	0.115/0.105
r^2	0.996/0.981	0.994/0.995	0.956/0.986	0.964/0.981	0.961/0.973	0.939/0.989
SD	0.037/0.023	0.069/0.071	0.054/0.062	0.071/0.072	0.025/0.047	0.069/0.056
DR						
q_m ($mg.g^{-1}$)	166/ 155	165/ 127	178/113	174/159	173/ 164	179/ 154
E^0 (KJ)	2.56/ 9.03	2.16/6.25	2.75/2.17	2.66/5.29	2.59/ 4.73	1.42/ 1.05
r^2	0.957/0.968	0.967/0.943	0.960/0.882	0.960/0.964	0.954/0.964	0.966/0.978
SD	0.092/0.043	0.093/0.068	0.074/0.079	0.077/0.059	0.051/0.044	0.050/0.077
Halsey						
$K_H(mg/g)(dm^3/mg)^{1/n}$	0.751/0.639	0.778/0.734	0.388/0.224	0.416/0.163	0.332/0.285	0.359/0.974
n_H	-0.94/-1.06	-0.95/-1.06	-1.03/-1.25	-1.04/-1.31	-1.11/-1.15	-0.69/-0.98
r^2	0.994/0.999	0.999/0.995	0.994/0.995	0.999/0.967	0.996/0.999	0.997/0.999
SD	0.090/0.088	0.047/0.022	0.079/0.071	0.032/0.048	0.052/0.027	0.029/0.084

Flori-Huggins						
$K_{FH}(mg/g)(dm^3/mg)^{1/n}$	1.174/ 1.6E-29	3.871/ 1.945E-12	1.426/ 4.197E-37	1.374/ 6.531E-16	1.384/ 2.884E+34	1.143/ 4.092E+18
N_{FH}	2.31/ -39.41	2.53/-19.18	2.56/-27.79	2.64/-14.57	2.61/-34.58	3.28/28.39
r^2	0.999/0.985	1.000/0.989	0.991/0.958	0.986/0.997	0.992/0.894	0.999/0.998
SD	0.025/0.025	0.002/0.071	0.099/0.011	0.061/0.049	0.072/0.025	0.087/0.042
Elovich						
q_m ($mg.g^{-1}$)	1.286/1.244	1.516/1.206	1.813/1.613	1.743/1.844	0.6340.466	0.891/0.954
K_E ($dm^3.mg^{-1}$)	9.23E+125/ 7.249E+85	8.959E+55/ 6.848E+85	5.195E+89/ 3.247E+80	7.443E+95/ 3.658E+46	1.37E+236/ 8.69E+190	7.89E+125/ 1.69E+54
r^2	0.994/0.932	0.924/0.999	0.985/0.997	0.967/0.991	0.911/0.950	0.989/0.945
SD	0.046/0.018	0.068/0.002	0.071/0.005	0.089/0.016	0.020/0.047	0.084/0.026
Cu^{2+}/ Hg^{2+}						
q_e (exp) ($mg.g^{-1}$)	36/239	42/218	125/220	88/217	117/206	33/230
Freundlich						
K_f ($L.g^{-1}$)	1.380/2.230	1.413/1.928	2.41/2.139	1.62/1.935	2.76/1.499	1.142/1.79
N	2.311/0.991	2.267/1.242	2.40/1.344	1.99/1.265	2.67/1.287	2.241/1.03
r^2	0.863/0.984	0.874/0.994	0.97/0.989	0.95/0.995	0.997/0.97	0.950/0.98
SD	0.023/0.040	0.023/0.034	0.013/0.03	0.02/0.017	0.004/0.01	0.013/0.02
Langmuir						
K_L ($L.mmol^{-1}$)	0.008/0.06	0.011/0.16	0.012/0.27	0.006/0.18	0.019/0.16	0.003/0.07
q_m ($mg.g^{-1}$)	40/105	45/ 35	119/30	99/34	120/23	40/60
ΔG ($kJ.mol^{-1}$)	-12.6/-7.22	-11.9/-4.68	-11.5/-3.4	-13.4/-4.5	-10.4/0.963	-14.7/-7.1
r^2	0.989/0.88	0.98/0.997	0.865/0.97	0.91/0.999	0.96/0.986	0.90/0.65
SD	0.078/0.02	0.02/0.015	0.415/0.06	0.069/0.01	0.07/0.11	0.672/0.09
Temkin						
$-\Delta H$ ($kJ.mol^{-1}$)	13.519/2.82	17.71/1.17	15.98/0.932	14.44/1.12	18.10/0.66	14.72/1.75
K_T ($L.mmol^{-1}$)	0.130/0.301	3.11/0.123	0.394/0.122	0.119/0.12	0.81/0.040	0.068/0.19
r^2	0.956/0.997	0.997/0.996	0.893/0.994	0.931/0.99	0.951/0.91	0.905/0.99
SD	0.087/0.037	0.065/0.097	0.074/0.085	0.039/0.08	0.021/0.04	0.065/0.09
DR						
q_m ($mg.g^{-1}$)	34/ 218	37/ 172	65/ 174	64/ 169	60/ 152	17/ 211
E_0 ($KJ.mol^{-1}$)	0.125/19.33	0.133/9.55	0.811/9.64	0.206/9.18	1.77/3.59	0.198/11.9
r^2	0.944/0.993	0.925/0.975	0.847/0.974	0.963/0.98	0.789/0.96	0.625/0.99
SD	0.047/0.090	0.048/0.066	0.081/0.071	0.033/0.09	0.077/0.08	0.045/0.07
Halsey						
k_H ($L.g^{-1}$)	0.182/0.16	0.165/0.152	0.01/0.09	0.108/0.15	0.002/0.30	0.505/0.25
n_H	-2.31/-0.99	-2.27/-1.25	-2.40/-1.34	-1.20/-1.27	-2.67/-1.29	-2.24/-1.03
r^2	0.863/0.984	0.874/0.994	0.971/0.99	0.947/0.81	0.997/0.97	0.95/0.98
SD	0.053/0.07	0.052/0.015	0.036/0.01	0.096/0.08	0.10/0.083	0.097/0.03
Flori-Huggins						
k_{fh} ($L.g^{-1}$)	0.001/ 1.380E-14	0.033/ 1.940E-05	0.024/ 0.0002	0.036/ 3.419E-05	0.009/ 1.370	0.01/ 3.97
n_{fh}	-3.86/-8.92	-1.416/-2.62	-2.34/-1.63	-1.09/-2.41	-15.45/4.38	-3.46/ 2.31
r^2	0.981/0.98	0.989/0.97	0.978/0.99	0.996/0.96	0.983/0.88	0.981/0.99
SD	0.023/0.06	0.038/0.08	0.092/0.02	0.079/0.02	0.078/0.03	0.063/0.08
Elovich						
q_m ($mg.g^{-1}$)	0.47/6.56	0.504/6.46	2.836/10.8	0.831/6.74	7.29/0.612	0.214/2.32
K_E ($L.mmol^{-1}$)	2644/ 5.5E+258	17703/ 2.3E+58	2.90E+53/ 5.54E+61	4.29E+15/ 3.29E+56	3.07E+94/ 2.96E+89	38.53/ 3.53E+116
r^2	0.756/0.88	0.768/0.999	0.817/0.96	0.812/0.99	0.939/0.99	0.775/0.99
SD	0.052/0.09	0.083/0.006	0.019/0.02	0.071/0.04	0.075/0.05	0.074/0.072

The Freundlich isotherm model fits the experimental data very well due to the heterogeneous distribution of non identical and energetically non uniform sites on the adsorbents under study. According to Treybal [44], an *n* value between 1 and 10 represents beneficial adsorption. The value of n, for the Freundlich model falling in the range of 0.98 to 1.34 for Cd^{2+}, Zn^{2+} and Hg^{2+}, 1.9 to 2.6 for Cu^{2+},indicates favorable adsorption. Langmuir equation relates the coverage of molecules on a solid surface to concentration of a medium above the solid surface at a fixed temperature. For the Langmuir model, the parameters K_L (equilibrium adsorption constant) and q_{max} were calculated from the intercept and slope of the plot of C_e/q_e versus C_e. For the Langmuir model r^2 varied from 0.86 to 0.998. In the present work although both the equations are obeyed, Freundlich isotherm model has a slightly better correlation coefficient and SD value indicating that surface of the adsorbents is heterogeneous in the long range but may have short range uniformity [45]. The comparative adsorption capacities were found in the order of $Cu^{2+}<Cd^{2+}\sim Zn^{2+}\sim Hg^{2+}$, adsorption capacity for Cu^{2+} was found to be lowest among the metal ions studied.

In case of Cd^{2+}, Cu^{2+} and Zn^{2+}, SAPSP, PAPSP was found to have better adsorption capacities, whereas for Hg^{2+} it was PSP. 9AAC showed higher adsorption capacities in case of Cu^{2+} and Zn^{2+} as compared to Cd^{2+} and Hg^{2+} due to the affinity of the hard copper and zinc to the hard basic ligands present in 9AAC. Higher adsorption of Hg^{2+} onto PSP as compared to other adsorbents may be due to the reduction of mercury to elemental mercury and creation of more carboxyl groups as seen from XPS studies in section 3.3.8. The correlation coefficients of Temkin model (0.893 to 0.996) indicate a satisfactory fit of the model to the experimental data. The variation of adsorption energy, ΔQ was found to be positive for all the metal ions adsorbed onto PSP, APSP, SAPSP, PAPSP, 9AAC and PAPSP, indicating the adsorption to be exothermic.

The Dubinin–Radushkevich model does not assume a homogeneous surface, like the Langmuir model. Its theory of filling the micro-pore volume is based on the fact that the adsorption potential is variable and that the free adsorption enthalpy is linked to the degree of pore filling. The values of correlation coefficients obtained from D-R model are lower than other isotherm values representing poor fit to experimental data and hence further analysis of D-R model was not done.

In all cases, though the Elovich isotherm exhibited good coefficients of correlation for the

adsorbents under study, the values of maximum adsorption capacity determined (Table 3.3) are lower than the experimental adsorbed amounts at equilibrium. Therefore, the Elovich model is unable to describe the adsorption isotherms of the metal ions onto all the adsorbents under study.

Multilayer adsorption is generally discussed by the Halsey equation and is found to fit well with the experimental data having r^2 ($\geq$ 0.865)[46] indicating that the mechanism may be multilayer adsorption for PSP, APSP, SAPSP, PAPSP, 9AAC and MPSP. However, the values of K_H suggest that multilayer adsorption might be playing only a small role.

The Flory-Huggins model was used to assess the isotherm data (Table 3.3). Though the correlation coefficients seem to be high, the negative value of n and low values of k_{FH} imply that the model cannot be used to describe the adsorption data. Thus it can be concluded that the Freundlich and Langmuir isotherm model fits best with low SD values followed by Halsey and Temkin. The adherence to these models suggests that these adsorbents might have homogeneous and heterogeneous surface energy distributions which would induce single and multilayer adsorption occurring either simultaneously or one after another.

3.3.4. Thermodynamic Parameters.

The negative value of ΔH^0 indicates that the adsorption of M^{2+} on PSP, APSP, SAPSP, PAPSP, 9AAC and MPSP is exothermic. The negative values of ΔG^0 in Table 3.4 indicate that the adsorption of M^{2+} by the adsorbents under study is by physisorption and is spontaneous and thermodynamically favorable [47]. The negative values of ΔS^0 are indicative of decrease in randomness during adsorption and a high affinity of the adsorbent towards the adsorbate.

Table 3.4. Thermodynamic Parameters for Cd^{2+}, Zn^{2+}, Cu^{2+} and Hg^{2+}

	Cd	Zn	Cu	Hg
		ΔG (KJ/mol)		
PSP	-1.849	-3.664	-0.612	-34.184
APSP	-3.124	-2.12	-8.583	-6.871
SAPSP	-2.304	-3.272	-4.571	-5.233
PAPSP	-3.001	-3.36	-3.152	-5.82
9AAC	-1.844	-2.814	-0.495	-9.765
MPSP	-2.451	-2.707	-0.632	-16.157
		ΔS (KJ/molK)		
PSP	0.0001	0.006	0.841	0.049
APSP	0.0009	0.002	13.302	0.009
SAPSP	0.0002	0.004	6.983	0.005
PAPSP	0.0019	0.003	4.714	0.008
9AAC	0.0001	0.004	0.665	0.015
MPSP	0.0019	0.004	0.829	0.022

ΔH (KJ/mol)				
PSP	-1.818	-1.922	-0.358	-19.241
APSP	-3.097	-1.601	-4.553	-4.1
SAPSP	-2.248	-2.206	-2.455	-3.663
PAPSP	-2.419	-2.38	-1.724	-3.533
9AAC	-1.812	-1.506	-0.294	-5.079
MPSP	-1.852	-1.415	-0.381	-9.395

3.3.5. Fourier Transform Infrared Spectroscopy.

Infrared spectra of the pristine and metal-loaded sorbents are shown in Figure 3.5. From figure 3.5 it is evident that there is shift in wave number and decrease in intensity of certain bands. Similarity in FTIR spectra of PSP with APSP and PAPSP suggests that a large proportion of the organic functional groups are retained on chemical or physical treatment of palm shell powder at 150^0C (Figure 3.5).

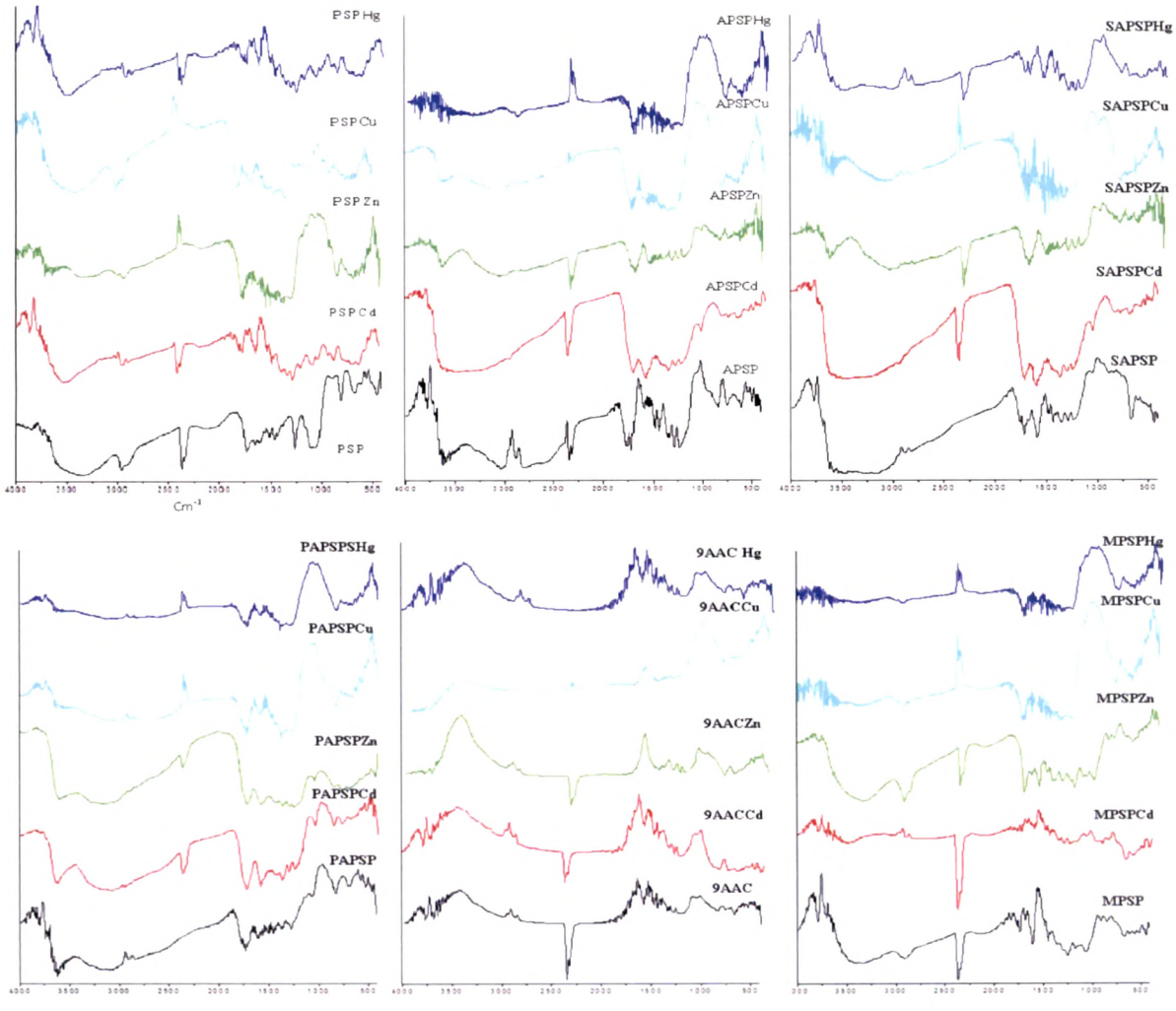

Figure 3.5. FTIR of native and metal loaded samples

Table 3.5. Typical Absorption frequencies and Carbonyl stretching frequencies of Infra red spectra for free and metal loaded adsorbents

PSP-Cd/Zn	APSP-Cd/Zn	SAPSP-Cd/Zn	PAPSP-Cd/Zn	9AAC-Cd/Zn	MPSP-Cd/Zn	Assignment
3451/3561	3450/3633	3478/ 3606	3621/3601	-	3496/ 3331	-N-H, -O-H stretching
2887, 2830/ 3244, 2889	2923/3002, 2896	3040, 2877/ 3074, 2896	3067, 2935/ 3153, 2894	2995, 2882/ 2995, 2870	2995, 2879/ 2923, 2855	$-CH_3$, $-CH_2$ symmetric stretch
2347/2131	2357/2353	2357/ 2359	2349/ 2357	2366/2357	2361/ 2369, 2119	Free CO_2
1717/1735	1709/1719	1716/ 1723	1716/ 1709	-	1716/ 1731	-C=O stretch for acids or aldehyde
1594/ 1599, 1520	1584/1572	1589/ 1580	1580/ 1573	1572/ 1574	1584/ 1585	-C=O stretch cellulose/ C=C Aromatic stretch (skeletal vibration)/ N-H bending of amide
1436/ 1460, 1416	1440/1433	1479, 1433/ 1433	1433/ 1433	1486, 1433/ 1486, 1433	1433/ 1452	$-CH_2$- stretch/ -C=C- Aromatic stretching
1346/1368	1361/1354	1347/ 1354	1354/ 1354	1342/ 1347	1347/ 1361	-C-H stretch/ N-H bending
1238/1263	1229/1229	1229/ 1237	1229/ 1229	1215/ 1227	1237/ 1229	-C-O bending of carboxylic acids/ phenolic O-H stretch/ N-H bending
1166/1118	-	-	-	-	1157/ 1162	-O-H stretch (2^0 Alcohol), -C-O-C- stretching
1049/1033	1042/1033	1045/ 1037	1033/ 1033	1064/ 1037	1052/1045	-C-H stretch, -C-O stretch (1^0 Alcohol)
893/893	-	-	-	-	894/ 894	Anomeric C-H bending of cellulose
845/845	826/853	841/ 834	-/ 834	841/ 841	841/ 841	-C-H out of plane bending
768, 549, 404/ 771, 512, 423	768, 572, 404/772, 526, 418	755, 549, 437, 409/ 764, 518, 423	762, 516, 404/ 778, 510, 422	750, 558, 493, 418/ 777, 512, 426	750, 535, 420/ 769, 516, 419	Cd/ Zn -O bending vibrations
PSP-Cu/Hg	**APSP-Cu/Hg**	**SAPSP-Cu/Hg**	**PAPSP-Cu/Hg**	**9AAC-Cu/Hg**	**MPSP-Cu/Hg**	**Assignment**
3352/3456	3606/ 3569	3645/ 3788, 3501	3612/ 3584	-/-	3304/3343	-N-H, -O-H stretching
2930/ 2943, 2875	3067/ 2920, 2875	3050/ 3056, 2867	3055/ 3079, 2883	3055/ -	2889/ 2953, 2880	$-CH_3$, $-CH_2$ symmetric stretch
1738/ 1758, 1713	1728/ 1728	1731/ 1766, 1728	1723/ 1728	-/-	1738/ 1735	-C=O stretch for acids or aldehyde
1603/ 1600	1589/ 1600	1556/ 1592	1528/ 1584	1587/ 1584	1644/ 1652, 1600	-C=O stretch cellulose/ C=C Aromatic stretch (skeletal vibration)/ N-H bending of amide
1428/ 1479, 1433	1436/ 1449	1436/ 1472, 1423	1428/ 1471	1428/ 1486, 1449	1450/ 1449	$-CH_2$- stretch/ -C=C- Aromatic stretching
1368/ 1335	1361/ 1366	1361/ 1350	1376/ 1373	1373/ 1350	1366/ 1350	-C-H stretch/ N-H bending
1261/ 1283	1294/ 1260	1289/ 1290	1285/ 1285	-/-	1268/ 1260	-C-O bending of carboxylic acids/ phenolic O-H stretch/ N-H bending
1040/ 1049	-/-	1021/ 1041	1028/ 1026	-/ 1049	-	-C-H stretch, -C-O stretch (1^0 Alcohol)
826/ 845	819/ 822	817/ 837	826/ 822	834/ 845	826/ 822	-C-H out of plane bending
797, 533, 425/ 790, 527	790, 536, 428/ 787, 524	789, 533, 427/ 792, 525	794, 530, 422/ 789, 527	780, 526, 420/ 793, 531	791, 528, 421/ 796, 530, 418	Cu/ Hg -O bending vibrations

The band at 3300- 3600 cm^{-1} represents -OH and -NH groups in the adsorbents under study (Table 3.5). The shift in the band to 3400-3650 cm^{-1} indicates M^{2+} –OH and –NH interaction during metal sorption onto the adsorbents under study. Carboxylate groups exhibit

bands in the range 1700-1732 and ~1200 cm^{-1} for the adsorbents under study. The bands were shifted to 1710-1735 and 1215-1265 cm^{-1} respectively in metal loaded adsorbents. This shift could be due to the association of the carbonyl group with metal ions [37]. The bands at 1125 cm^{-1}-1127 cm^{-1} could be due to the –C–O stretching of ether groups while the bands at 1030 cm^{-1}-1065 cm^{-1} could be assigned to the –C–O stretching of alcoholic groups. The difference between C=O and C-O bond stretching has been related to the relative symmetry of these two carbon-oxygen bonds and is reported to reflect the nature of carboxyl group binding status [48].

Adsorbents were found to have much larger Δ values than the metal loaded adsorbents (Table 3.6). The lower values of Δ in the presence of metal ions indicate the involvement of carboxylate groups in forming complexes with metal ions.

Table 3.6. Δ values for virgin and metal loaded adsorbents

Biosorbent	$\upsilon_{C=O}$	υ_{C-O}	$\Delta = \upsilon_{C=O} - \upsilon_{C-O}$	**Biosorbent**	$\upsilon_{C=O}$	υ_{C-O}	$\Delta = \upsilon_{C=O} - \upsilon_{C-O}$
PSP	1732	1250	482	PAPSP	1723	1235	488
APSP	1720	1229	491	MPSP	1727	1238	489
SAPSP	1723	1229	494				
PSP-Cd	1717	1238	479	PSP-Zn	1735	1263	472
APSP-Cd	1709	1229	480	APSP-Zn	1719	1229	490
SAPSP-Cd	1716	1229	487	SAPSP-Zn	1723	1237	486
PAPSP-Cd	1716	1229	487	PAPSP-Zn	1709	1229	480
MPSP-Cd	1716	1237	479	MPSP-Zn	1731	1229	502
PSP-Cu	1738	1261	477	PSP-Hg	1758	1283	475
APSP-Cu	1728	1294	434	APSP-Hg	1728	1260	468
SAPSP-Cu	1731	1289	442	SAPSP-Hg	1766	1290	476
PAPSP-Cu	1723	1285	438	PAPSP-Hg	1728	1285	443
MPSP-Cu	1738	1268	470	MPSP-Hg	1735	1260	475

It is clear from the FT-IR analysis that the possible mechanism of adsorption of Cd^{2+}, Zn^{2+}, Cu^{2+} and Hg^{2+} on the adsorbents may be physical adsorption, ion exchange, surface precipitation, complexation with functional groups and chemical reactions with surface sites [49, 50].

3.3.6. Column Studies.

The column breakthrough curves for Cd^{2+}, Zn^{2+}, Cu^{2+} and Hg^{2+} are shown in Figure 3.6. The effluent concentration is seen to have the typical 'S' shape.

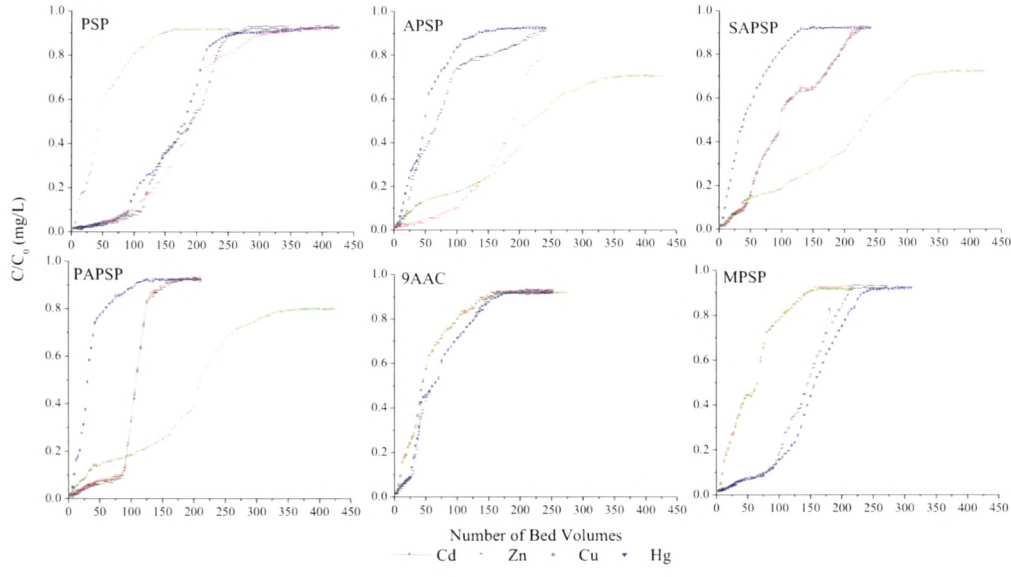

Figure 3.6. Column breakthrough studies

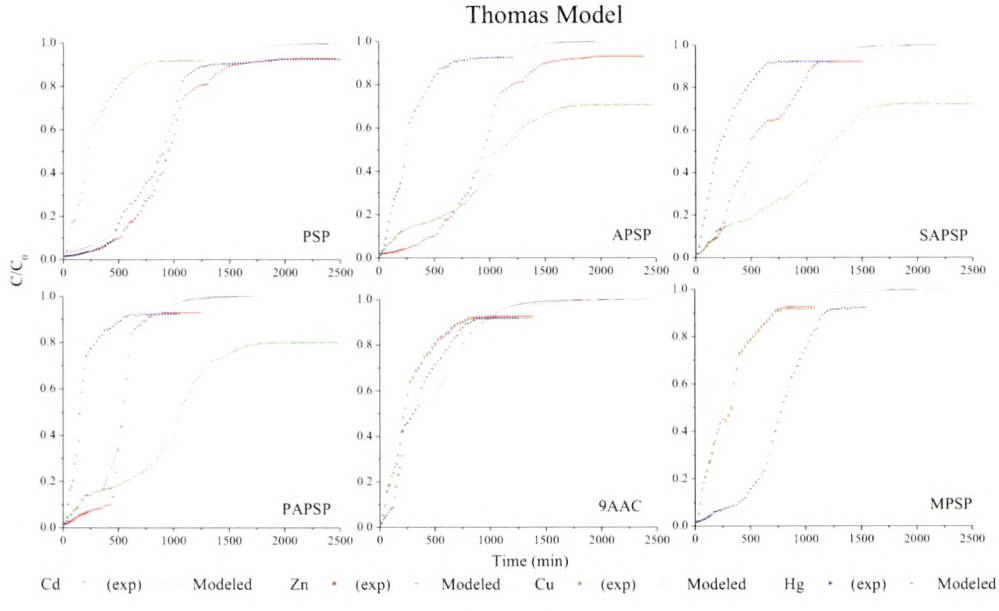

Figure 3.7. Thomas Model for for Cu^{2+}, Cd^{2+}, Zn^{2+} and Hg^{2+}

Thomas and Yoon–Nelson models were also applied to the column adsorption data at a flow rate of 1mL/min at an initial metal ion concentration of 1g/L and bed height 5cm for M^{2+} with all the adsorbents under study. The respective values of Thomas rate constant (k_{Th}) and bed capacity (q_{Th}) were calculated from the linear plots of $\ln[(C_o/C_t)-1]$ versus V_{eff}. The theoretical predictions based on the model parameters are compared in Figure 3.7 with the observed data. The well fit of the experimental data on to the Thomas model indicate that external and internal diffusion will not be the limiting step.

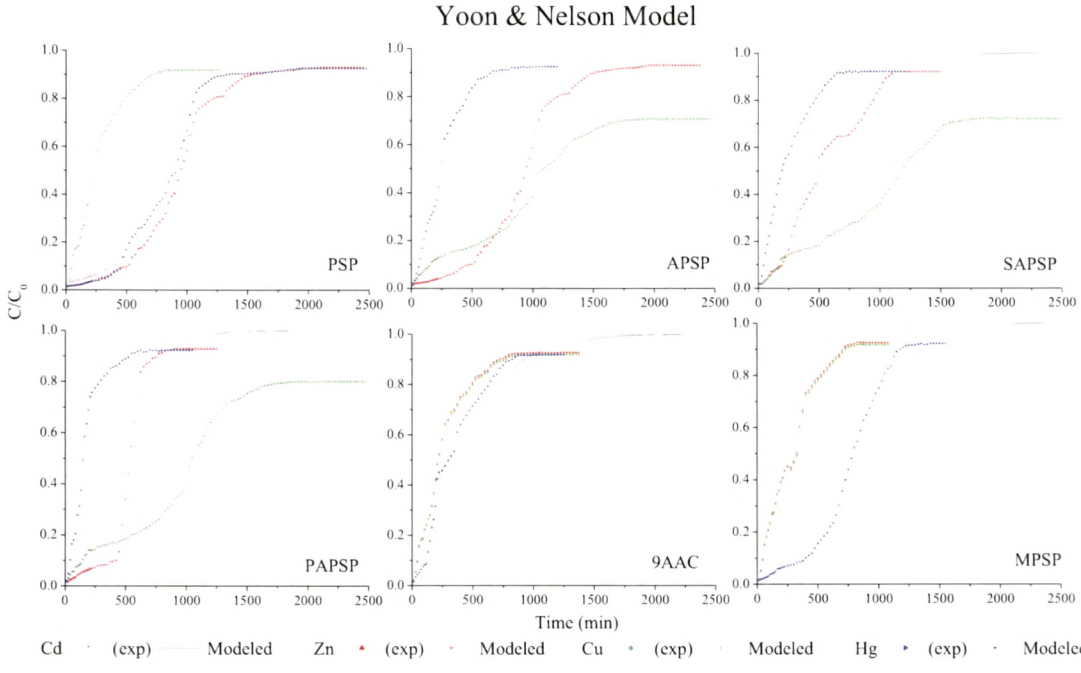

Figure 3.8. Yoon & Nelson Model for Cu^{2+}, Cd^{2+}, Zn^{2+} and Hg^{2+}

It can be seen that the less stirred property in column mode reduces the M^{2+} adsorption capacity of PSP, APSP, SAPSP, PAPSP, 9AAC and MPSP. The trend observed in maximum adsorption capacity measured in batch system is different from that measured in columns as the diffusion coefficient is different in batch and column reactors and is also dependent on flow rate in column [51]. From the equations in Table 3.1 it is evident that the characteristic parameter associated with Thomas and Yoon and Nelson models (Figure 3.8) vary but both the models predict essentially same uptake capacity and C/C_0 values for a particular experimental set of data. Hence same r^2 and SD values were obtained as also suggested by Baral et al. [52].

3.3.7. Desorption studies.

Solutions of 0.1 N HCl, 0.1 N EDTA and 0.1 N NH_3 have been studied as eluents for desorption of M^{2+}.

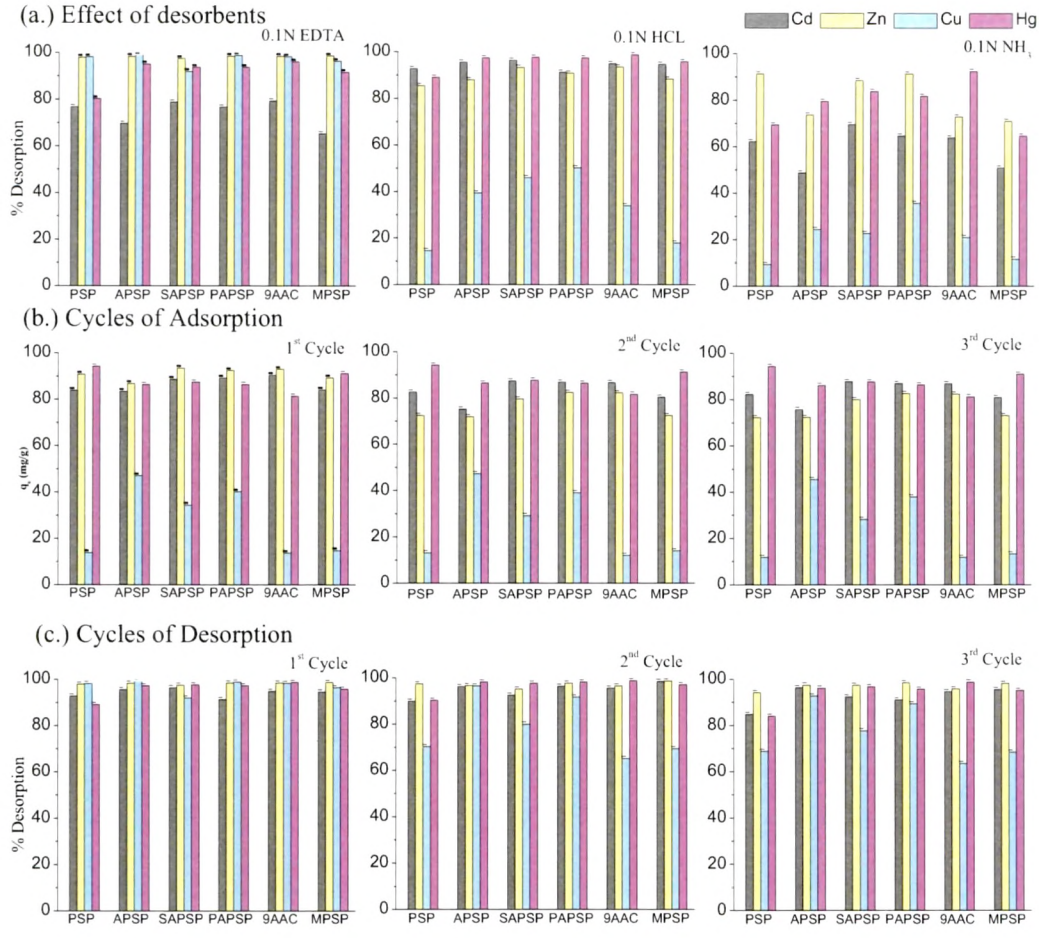

Operating parameters: Adsorption: 30 ^{0}C, 180 min, optimum pH, 1000 ppm, 0.1 g adsorbent, 180 rpm. Desorption: 0.1 N eluent, 30 ^{0}C.

Figure 3.9. Desorption and cycles of adsorption: a)Effect of desorbents, b) Cycles of adsorption, c) Cycles of desorption for Cu^{2+}, Cd^{2+}, Zn^{2+} and Hg^{2+}

From Figure 3.9 it is evident that desorption of Cd^{2+} and Zn^{2+} from the metal-loaded adsorbents with 0.1M HCl and 0.1M EDTA resulted in greater than 92 and 99% recovery of these metals, respectively. It was observed that Cd(II) and Zn(II) were easily desorbed within 30

min, which would prove highly advantageous for metal recovery. It is also seen that the removal capacity of adsorbents decreased only by ~6% in the second cycle, and by ~6.5% in the third cycle. Quantitative desorption of Cd(II) and ~86% desorption of Zn(II) with HCl suggests that the metal ions are adsorbed to the functional groups of the adsorbents under study by electrostatic attraction while ~79% desorption of Cd(II) and quantitative desorption of Zn(II) with 0.1N EDTA could be due to the stability of Cd-EDTA ($2.9x10^{16}$) and Zn-EDTA ($3.2x10^{16}$) chelates.

HCl desorbed 16-42% of Cu^{2+} from the adsorbents under study while NH_3 desorbed 10-38% of Cu^{2+}. On the other hand EDTA was found to be effective in desorbing >95% of copper from all the adsorbents under study. The adsorbents exhibited highest copper uptake capacities for PAPSP (48, 48 and 47 mg/g in first, second and third cycles, respectively). In the case of APSP and PAPSP 0.1M EDTA maintained a consistent elution efficiency of around 100, 98, 97% in the first second and third desorption cycle respectively. Such high elution efficiency with EDTA could be due to high stability constants of Cu-EDTA complexes.

From Figure 3.9 it is evident that desorption of Hg^{2+} from the metal-loaded PSP with 0.1M HCl resulted with ~90% recovery. However, the use of 0.1M EDTA and 0.1 M NH_3 resulted in 81.2 and 70.2 % recovery of Hg^{2+} respectively. It was observed that mercury was easily desorbed within 30 min, which would prove highly advantageous for metal recovery. This indicates that ion exchange is involved in the adsorption process [53].

It was observed that all the metal ions were easily desorbed within 30 min, which would prove highly advantageous for metal recovery. Thus regeneration and reuse of the adsorbents under study was checked for 3 cycles and found to be an economical and efficient method for removal of M^{2+} from water.

3.3.8. X-ray Photoelectron Spectroscopy.

The wide scan XPS spectra of adsorbents (native and metal-loaded adsorbents) are presented in Figure 3.10,deconvoluted spectra in Figures 3.11 and 3.12 and the corresponding binding energies with relative content of species studied are listed in Table 3.7. X-ray photoelectron spectroscopy was employed to study the binding energy (BE) of oxygen (O1s), carbon (C1s), nitrogen (N1S) in adsorbents under study and to study the shift in binding energy after mercury and copper adsorption.

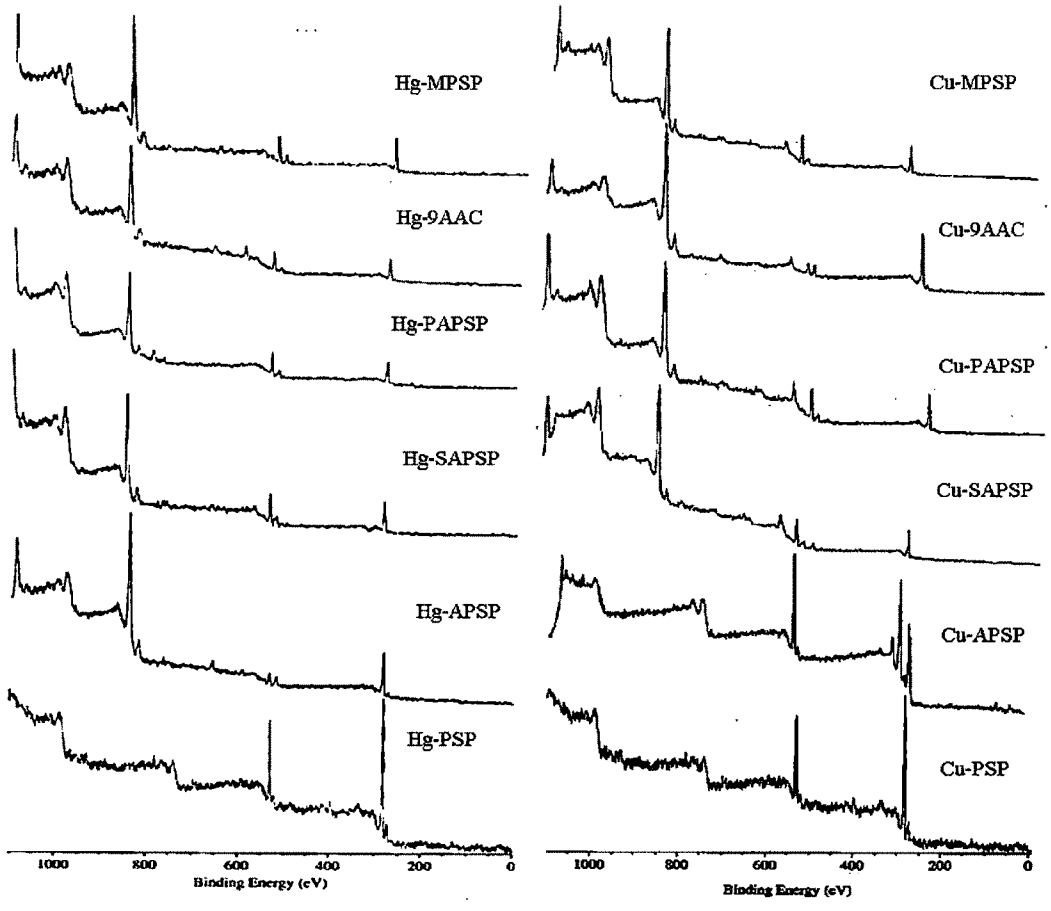

Figure 3.10. Wide scan spectra for Cu^{2+} and Hg^{2+}

The changes in the contents of C=O and C-O after metal adsorption indicate that, these groups are involved in the adsorption of metal onto the adsorbents, which is consonant with the FT-IR analysis

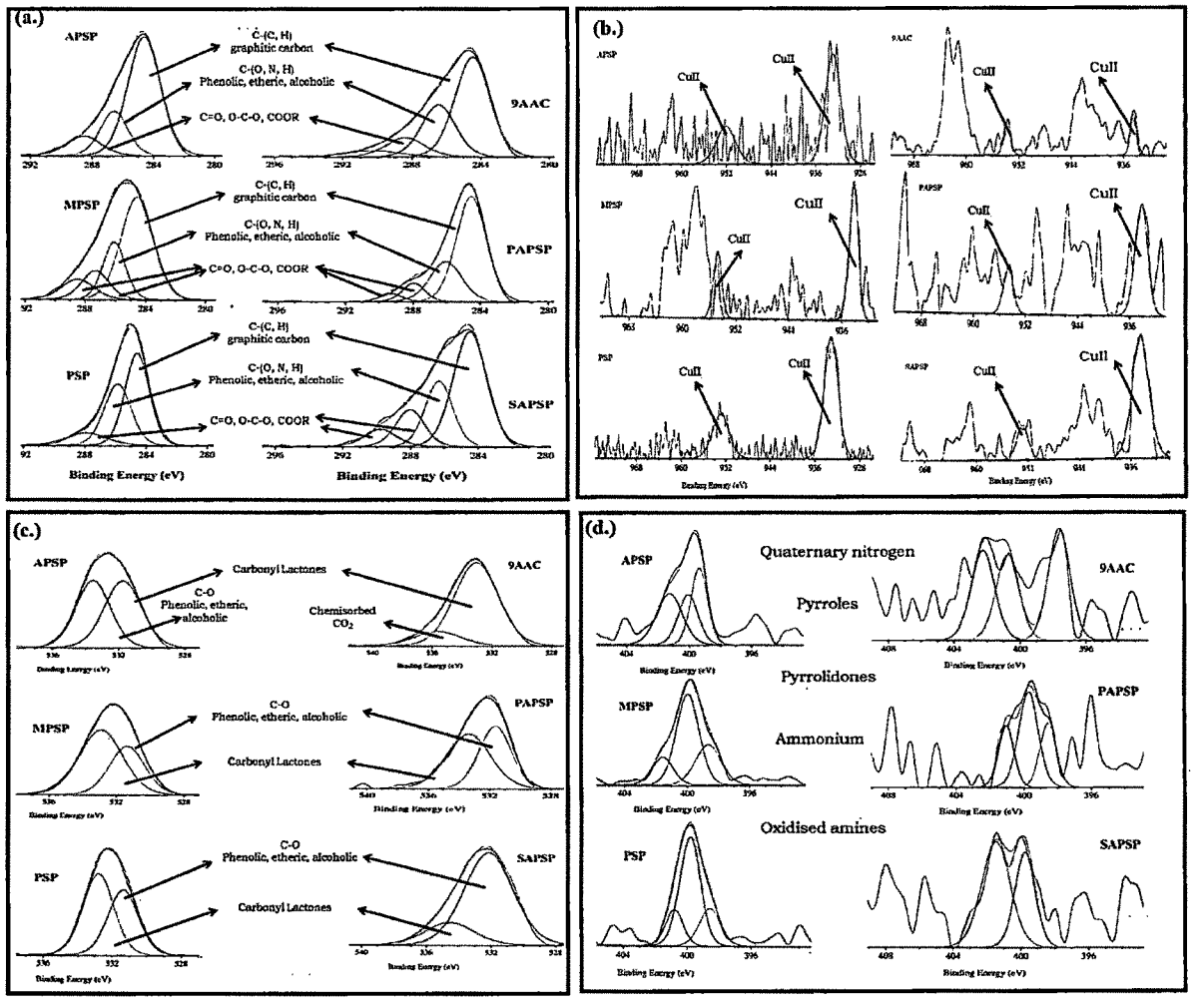

Figure 3.11. Deconvoluted (a.) C1s spectra (b.) Cu2p spectra (c.) O1s spectra and (d.) N1s spectra for the Cu-loaded adsorbents

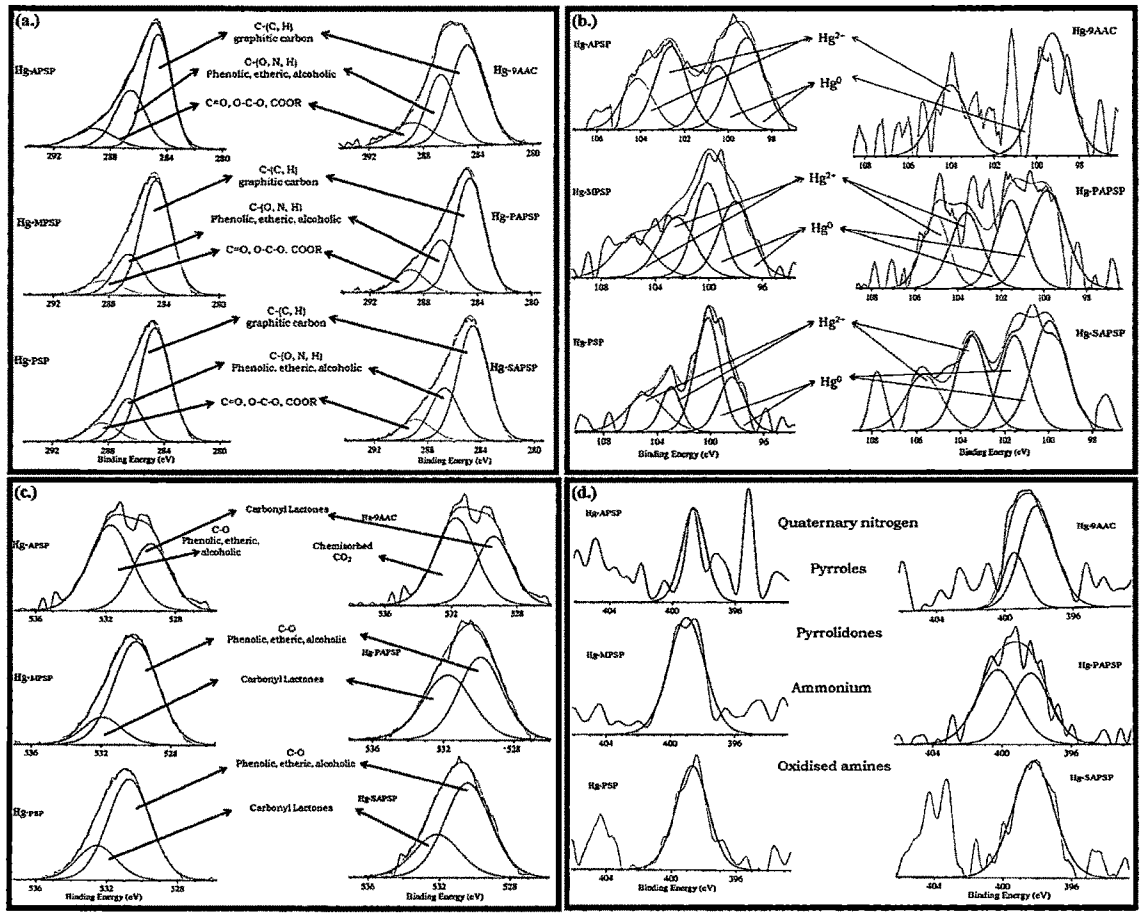

Figure 3.12. Deconvoluted (a.) C1s spectra (b.) Cu2p spectra (c.) O1s spectra and (d.) N1s spectra for the Hg-loaded adsorbents

Table 3.7. Summary of binding energy and area ratios of pristine and Cu^{2+} & Hg^{2+}-loaded sorbents

Sample Surface	Proposed components	Binding Energy(eV)	FWHM	Relative Quantity
C1s Valence State				
PSP	C-(C, H) graphitic C	284.661	2.310	0.6906
	C-(O, N, H) phenolic, alcoholic, etheric	285.984	1.774	0.1871
	C=O, O-C-O, COOR -carbonyl or quinine	287.200	2.495	0.1223
Hg-PSP	C-(C, H)	284.642	2.504	0.6639
	C-(OH, OR)	286.569	2.196	0.2209
	O=C-O carboxyl or ester	288.442	2.624	0.1152
Cu-PSP	C-(C, H)	284.570	1.899	0.6685
	C-(OH, OR)	286.183	1.663	0.2264
	O=C-O carboxyl or ester	287.881	2.186	0.1051
APSP	C-(C, H)	284.647	2.462	0.6716
	C-(OH, OR)	286.599	2.074	0.2112
	O=C-O	288.577	2.605	0.1172
Hg-APSP	C-(C, H)	284.696	2.206	0.5529
	C-(OH, OR)	286.605	2.550	0.3179
	O=C-O	289.188	3.139	0.1291
Cu-APSP	C-(C, H)	284.590	2.118	0.5491
	C-(OH, OR)	286.321	2.562	0.3086

	O=C-O	288.894	3.896	0.1263
SAPSP	C- (C, H)	284.524	2.264	0.5272
	C-(OH, OR)	286.342	1.894	0.2499
	O=C-O	288.073, 289.791	1.973, 2.181	0.1471, 0.0758
Hg-SAPSP	C- (C, H)	284.645	2.634	0.6139
	C-(OH, OR)	286.762	2.543	0.2700
	O=C-O	288.874	2.706	0.1151
Cu-SAPSP	C-(C, H)	284.682	2.374	0.4528
	C-(OH, OR)	286.275	2.331	0.3219
	O=C-O	288.115, 289.936	2.180, 2.467	0.1537, 0.0717
PAPSP	C-(C, H)	284.590	2.051	0.6297
	C-(OH, OR)	286.071	2.204	0.2552
	C=O, O-C-O, COOR	287.979	1.527	0.0817
	O=C-O	289.308	1.424	0.0334
Hg-PAPSP	C-(C, H)	284.620	2.510	0.5989
	C-(OH, OR)	286.738	2.576	0.2819
	O=C-O	289.023	2.515	0.1191
Cu-PAPSP	C-(C, H)	284.581	2.367	0.4962
	C-(OH, OR)	286.119	2.337	0.2895
	C=O, O-C-O, COOR	287.957	2.502	0.1621
	O=C-O	289.802	2.602	0.0521
9AAC	C-(C, H)	284.507	2.336	0.5552
	C-(OH, OR)	286.511	2.284	0.2822
	C=O, O-C-O, COOR	288.384	2.572	0.1155
	C=C, occluded CO, π electrons in aromatic ring, CO_2	290.295	3.464	0.0471
Hg-9AAC	C-(C, H)	284.665	2.935	0.5300
	C-(OH, OR)	286.660	2.513	0.3209
	C=O, O-C-O, COOR	288.806	3.483	0.1481
Cu-9AAC	C-(C, H)	284.566	2.507	0.6918
	C-(OH, OR)	286.472	2.352	0.1744
	O=C-O	288.556	2.360	0.0829
	C=C, occluded CO, π electrons in aromatic ring, CO_2	290.939	3.606	0.0509
MPSP	C-(C, H, R), C-(C, H)	284.624	2.460	0.5456
	C-(OH, OR)	286.116, 286.346	1.718, 2.120	0.2137, 0.1311
	C=O, O-C-O, COOR O=C-O	288.517	2.491	0.1095
Hg-MPSP	C-(C, H, R), C-(C, H)	284.621	2.528	0.6759
	C-(OH, OR)	286.573	2.380	0.2260
	C=O, O-C-O, COOR O=C-O	288.391	2.907	0.9801
Cu-MPSP	C-(C, H, R), C-(C, H)	284.634	2.606	0.4712
	C-(OH, OR)	286.237	2.208	0.3381
	C=O, O-C-O COOR	287.650	1.517	0.1122
	O=C-O	289.142	1.897	0.0785
O1s Valence State				
PSP	C=O, C-O (Lactones, phenolic and etheric)	531.400	2.050	0.4424
	Singly bonded oxygen C-O	532.846	2.072	0.5576
Hg-PSP	C=O, C-O(Lactones, phenolic and etheric)	530.749	2.751	0.7579
	Singly bonded oxygen C-O	532.546	2.563	0.2521
Cu-PSP	C=O, C-O(Lactones, phenolic and etheric)	531.416	2.137	0.4460
	Singly bonded oxygen C-O	532.843	2.023	0.5539
APSP	C=O, C-O (Lactones, phenolic and etheric)	531.770	2.606	0.8160
	Singly bonded oxygen C-O	533.570	2.394	0.4796
Hg-APSP	C=O, C-O (Carboxylic acid, etheric, lactonic, anhydrides,	530.216	3.481	0.7579

	pyrones and phenols)	532.568	2.929	0.2421
Cu-APSP	C=O, C-O(Lactones, phenolic and etheric)	531.417	2.315	0.4934
	Singly bonded oxygen C-O	533.252	2.402	0.5067
SAPSP	C=O (Carboxylic acid)	532.209, 534.596	3.492, 3.517	0.8032, 0.1968
Hg-SAPSP	C=O, C-O (Carboxylic acid, etheric, lactonic, anhydrides, pyrones and phenols)	530.410, 532.119	2.987, 2.988	0.6869 0.3130
Cu-SAPSP	C=O, C-O (Carboxylic acid, etheric, lactonic, anhydrides, pyrones and phenols)	531.859 533.815	3.167 3.150	0.6953 0.3047
PAPSP	C=O, C-O (Carboxylic acid, etheric, lactonic, anhydrides, pyrones and phenols)	531.656 533.388	2.449 3.347	0.4576 0.5424
Hg-PAPSP	C=O, C-O (Carboxylic acid, etheric, lactonic, anhydrides, pyrones and phenols)	529.915 531.754	2.888 3.263	0.5321 0.4680
Cu-PAPSP	C=O, C-O (Carboxylic acid, etheric, lactonic, anhydrides, pyrones and phenols)	531.935 533.832	2.771 2.781	0.6274 0.3726
9AAC	C=O, C-O (Carboxylic acid, etheric, lactonic, anhydrides, pyrones and phenols)	533.080	3.389	0.8437
	Occluded CO, chemisorbed CO_2, O_2 and H_2O	535.638	3.618	0.1563
Hg-9AAC	C=O, C-O (Carboxylic acid, etheric, lactonic, anhydrides, pyrones and phenols)	529.434 531.736	2.518 2.851	0.4085 0.5910
Cu-9AAC	C=O, C-O (Carboxylic acid, etheric, lactonic, anhydrides, pyrones and phenols)	531.586 533.576	3.039 3.071	0.6443 0.3557
MPSP	C=O, C-O (Carboxylic acid, etheric, lactonic, anhydrides, pyrones and phenols)	531.367 532.931	2.440 2.978	0.3795 0.6205
Hg-MPSP	C=O, C-O (Carboxylic acid, etheric, lactonic, anhydrides, pyrones and phenols)	530.044 532.934	2.893 2.577	0.8089 0.1911
Cu-MPSP	C=O, C-O (Carboxylic acid, etheric, lactonic, anhydrides, pyrones and phenols)	531.497 533.075	2.757 2.798	0.5732 0.4268
N1S				
PSP	C-N-C (pyrrolic nitrogen, pyridines)	399.839, 398.597, 400.846	1.492, 1.512, 1.258	0.6129, 0.2141, 0.1729
Hg-PSP	C-N-C (pyrrolic nitrogen, pyridones)	398.759	2.317	1.000
Cu-PSP	C-N-C (pyrrolic nitrogen, pyridones)	399.182, 400.207	1.578, 2.038	0.3922, 0.6078
APSP	C-N-C (pyrrolic nitrogen, pyridones)	399.98, 400.075	1.228, 1.468	0.3556, 0.2780
	Quartenary nitrogen, protonated pyridinic ammonium ions, nitrogen atoms replacing carbon in graphene	401.278	1.908	0.3664
Hg-APSP	C-N-C (pyrrolic nitrogen, pyridones)	398.658	1.734	1.000
	Quartenary nitrogen, protonated pyridinic ammonium ions, nitrogen atoms replacing carbon in graphene	401.278	1.908	0.3664
Cu-APSP	C-N-C (pyrrolic nitrogen, pyridones)	400.028	1.824	0.6157
	Oxidised nitrogen functionalities or NO_2 groups	402.307	1.486	0.3843
SAPSP	C-N-C (pyrrolic nitrogen, pyridones)	399.797	1.366	0.3883
	Quartenary nitrogen, protonated pyridinic ammonium ions, nitrogen atoms replacing carbon in graphene	401.477	1.941	0.6118
Hg-SAPSP	C-N-C (pyrrolic nitrogen, pyridones)	398.237	2.747	1.000
Cu-SAPSP	C-N-C (pyrrolic nitrogen, pyridones)	400.073	1.753	0.7105
	Quartenary nitrogen, protonated pyridinic ammonium ions, nitrogen atoms replacing carbon in graphene	401.567	1.403	0.2895
PAPSP	C-N-C (pyrrolic nitrogen, pyridones)	398.584, 399.774	1.097, 1.319	0.2677, 0.4869

	Quartenary nitrogen, protonated pyridinic ammonium ions, nitrogen atoms replacing carbon in graphene	401.074	1.032	0.2454
Hg-PAPSP	C-N-C (pyrrolic nitrogen, pyridones)	398.348, 400.289	2.603, 2.781	0.4710, 0.5291
Cu-PAPSP	C-N-C (pyrrolic nitrogen, pyridones)	399.928	1.824	0.6157
	Oxidised nitrogen functionalities or NO_2 groups	402.207	1.486	0.3843
9AAC	C-N-C (pyrrolic nitrogen, pyridones)	397.686, 400.803	1.516, 1.596	0.3000, 0.3745
	Oxidised nitrogen functionalities or NO_2 groups	402.300	1.639	0.3255
Hg-9AAC	C-N-C (pyrrolic nitrogen, pyridones)	398.022, 399.356	1.516, 1.596	0.7319, 0.2681
Cu-9AAC	C-N-C (pyrrolic nitrogen, pyridones)	397.100, 399.700	1.326, 1.342	0.4173, 0.3199
	Quartenary nitrogen, protonated pyridinic ammonium ions, nitrogen atoms replacing carbon in graphene	401.400	1.199	0.2627
MPSP	C-N-C (pyrrolic nitrogen, pyridones)	398.703, 400.000	1.889, 1.679	0.2787, 0.5613
	Quartenary nitrogen, protonated pyridinic ammonium ions, nitrogen atoms replacing carbon in graphene	401.606	1.570	0.1599
Hg-MPSP	C-N-C (pyrrolic nitrogen, pyridones)	398.999	2.583	1.000
Cu-MPSP	Quartenary nitrogen, protonated pyridinic ammonium ions, nitrogen atoms replacing carbon in graphene	401.191	1.587	0.1034
	C-N-C (pyrrolic nitrogen, pyridones)	398.641, 399.939	2.160, 1.332	0.5294, 0.3672
Hg-PSP	Hg-4f 5/2 (Hg^0)	98.460	2.279	0.2169
	Hg-4f 5/2 (Hg^0)	102.985	1.733	0.1359
	Hg-4f 7/2 (Hg^{+2})	100.303	2.155	0.4310
	Hg-4f 7/2 (Hg^{+2})	104.878	3.366	0.2170
Cu-PSP	Cu-2p3/2 (Cu^{+2})	933.100	2.200	0.8685
	Cu-2p1/2 (Cu^{+2})	952.991	1.578	0.1324
Hg-APSP	Hg-4f 5/2 (Hg^0)	99.191	1.859	0.3399
	Hg-4f 5/2 (Hg^0)	102.626	1.680	0.2780
	Hg-4f 7/2 (Hg^{+2})	100.499	1.688	0.2130
	Hg-4f 7/2 (Hg^{+2})	104.153	1.665	0.1681
Cu-APSP	Cu-2p3/2 (Cu^{+2})	932.982	3.181	0.7000
	Cu-2p1/2 (Cu^{+2})	952.160	3.982	0.2999
Hg-SAPSP	Hg-4f 5/2 (Hg^0)	99.950	1.858	0.3359
	Hg-4f 5/2 (Hg^0)	103.531	1.564	0.2457
	Hg-4f 7/2 (Hg^{+2})	101.533	1.539	0.2422
	Hg-4f 7/2 (Hg^{+2})	105.678	1.909	0.1761
Cu-SAPSP	Cu-2p3/2 (Cu^{+2})	934.419	3.020	0.8431
	Cu-2p1/2 (Cu^{+2})	952.875	1.981	0.1569
Hg-PAPSP	Hg-4f 5/2 (Hg^0)	99.899	2.011	0.3429
	Hg-4f 5/2 (Hg^0)	103.653	1.691	0.2230
	Hg-4f 7/2 (Hg^{+2})	101.547	1.633	0.2501
	Hg-4f 7/2 (Hg^{+2})	105.092	1.441	0.1839
Cu-PAPSP	Cu-2p3/2 (Cu^{+2})	934.441	2.216	0.7536
	Cu-2p1/2 (Cu^{+2})	954.836	1.694	0.2473
Hg-9AAC	Hg-4f 5/2 (Hg^0)	99.273	1.842	0.6319
	Hg-4f 7/2 (Hg^{+2})	104.068	1.854	0.3680
Cu-9AAC	Cu-2p3/2 (Cu^{+2})	934.521	1.106	0.5370
	Cu-2p1/2 (Cu^{+2})	953.845	1.193	0.4629
Hg-MPSP	Hg-4f 5/2 (Hg^0)	98.088	2.816	0.2809
	Hg-4f 5/2 (Hg^0)	102.420	3.084	0.2440
	Hg-4f 7/2 (Hg^{+2})	100.122	2.385	0.2959
	Hg-4f 7/2 (Hg^{+2})	105.610	3.419	0.1791
Cu-MPSP	Cu-2p3/2 (Cu^{+2})	934.400	1.582	0.6949
	Cu-2p1/2 (Cu^{+2})	954.849	1.405	0.3050

Table 3.8. Surface concentration of oxygen containing carbon and graphitic carbon, % content of C, N and O

Samples	Cox/Cg	Surface concentration (from C 1s peak)%				
Native		C in graphite	Phenol-ether	Carbonyl-quinone	Carboxyl	Others
Hg-PSP	0.506	66.39	22.09	-	11.52	-
Hg-APSP	0.808	55.29	31.79	-	12.91	-
Hg-SAPSP	0.627	61.39	27.00	-	11.51	-
Hg-PAPSP	0.669	59.89	28.19	-	11.91	-
Hg-MPSP	0.479	67.59	22.60	-	9.80	-
Hg-9AAC	0.884	53.00	32.09	-	14.81	-
Cu-PSP	0.234	81.1	14.9	4.0	-	-
Cu-APSP	0.959	54.91	30.86	-	12.63	-
Cu-SAPSP	1.208	45.28	32.19	15.37	7.17	-
Cu-PAPSP	1.015	49.62	28.95	16.21	5.21	-
Cu-MPSP	1.122	47.12	33.81	11.22	7.85	-
Cu-9AAC	0.446	69.18	17.44	-	8.29	5.09
Native	**XPS (C, N, O)**	**O/ C ratio**	**Cu-Loaded**	**XPS (C, N, O)**		**O/ C ratio**
Hg-PSP	49.43, 1.39, 49.18	0.995	**Cu-PSP**	54.48, 1.74, 43.79		0.804
Hg-MPSP	54.54, 1.07, 44.39	0.814	**Cu-MPSP**	50.07, 1.62, 48.30		0.965
Hg-APSP	68.82, 0.39, 30.79	0.448	**Cu-APSP**	50.58, 0.49, 48.93		0.967
Hg-SAPSP	46.44, 1.58, 51.98	1.119	**Cu-SAPSP**	49.64, 0.58, 49.79		1.003
Hg-PAPSP	43.46, 3.18, 53.36	1.228	**Cu-PAPSP**	51.03, 0.49, 48.48		0.950
Hg-9AAC	53.89, 1.10, 45.00	0.835	**Cu-9AAC**	61.57, 0.68, 37.75		0.613

Table 3.8 shows changes in the contents of C=O and C-O after copper and mercury adsorption suggesting that these groups are involved in the adsorption of the metal ions onto the adsorbents, which is in consonance with the FT-IR results. The 2*p*3/2 peak of copper was fitted by binding energies corresponding to 933.1, 932.982, 934.419, 934.441, 934.521 and 934.400 for PSP, APSP, SAPSP, PAPSP, 9AAC and MPSP. The peaks for Cu^{2+} in Cu-PSP and Cu-APSP could be characterized as the Cu^{2+} that has relatively higher electron density in its valence shell, and the corresponding peaks in Cu-SAPSP, Cu-PAPSP, Cu-9AAC and Cu-MPSP as the Cu^{2+} ion with lower electron density in its valence shell. Cu^{2+} can gain electrons from the ligands (hydroxyl and ether) via covalent bonding while Cu^{2+} located in the ionic bonding environment (carboxylate) has less electron density. As a result, the Cu^{2+} ions in the former environment gave rise to a peak around ~933 eV and those in the latter one the peak about 934.0 eV. These observations suggested that the adsorption interactions of copper species might involve not only the cation exchange interaction resulted from the oxygen containing functional groups, there should be other interactions like complex formation. Thus the influence of the chemical

interaction of copper with surface functional groups in different environments has resulted in different binding energies for Cu^{2+} on the adsorbents under study. A corresponding shift in C1S peaks and O1S peaks is also observed

The XPS spectrum of copper treated adsorbents under study does not indicate any reduction whereas in case of mercury it showed reduction of Hg^{+2} to metallic mercury simultaneously oxidizing the adsorbent surface. The surface groups were divided for the adsorbents under study by taking their percentage in the surface layer from XPS data (C 1s peak was taken into account, following the procedure presented in [54]), as shown in Table 3.8. A relatively stronger intense peak at a BE of 398.759 eV indicates that the N-atoms existed in a more reduced state on the surfaces of adsorption due to mercury adsorption. This may be due to the formation of the covalent bond of N-Hg in which, Hg shared electrons with the N-atom, which increased the electron cloud density of the nitrogen atom and resulted in a lower BE peak observed. Deconvoluted XPS spectra of mercury in the Hg 4f region and the peaks at 99.779 and 103.949 eV correspond to the binding energies (4f7/2 and 4f 5/2) of elemental mercury [55]. On the other hand, the peaks at 100.303 and 104.878 eV correspond to the binding energies (4f7/2 and 4f 5/2) of Hg(II) in HgO [56] suggesting that part of the mercury on PSP is present in elemental form and partly in +2 state. An increase in the O/C ratio is observed which can be attributed to the oxidation of lignin aromatic carbons (aldehydic groups) by Hg(II) and formation of alcoholic sites, carboxylic sites and elemental mercury. Similar observation has been made by Dupont et al. during their studies on the removal of hexavalent chromium with a lignocellulosic substrate extracted from wheat bran [57] which could be related to the abundance of lignin and fatty acid moieties, which allow the reduction of Hg(II) into Hg(0) on carboxylic moieties [58]. Earlier studies reflected the binding of mercury on the biomass occurs through electrostatic and complexation reactions [59, 60].

3.3.9. Solid state-^{13}CNMR Spectroscopic Analysis.

^{13}C NMR spectral analysis was done only for copper loaded samples as a representative to see the changes occurring in the adsorbents after metal adsorption.^{13}C solid state NMR spectra of Cu-loaded adsorbents is presented in Figure 3.13, the peaks assigned to different carbons are shown in Table 3.9.

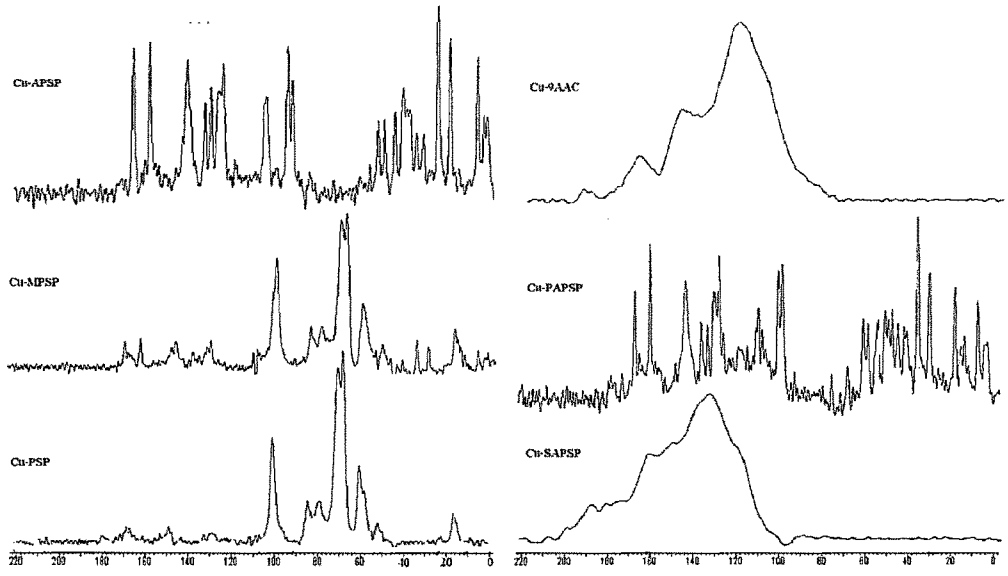

Figure 3.13. NMR spectra for the Cu-loaded adsorbents

Table 3.9. Assignments to the NMR peaks

PSP	Cu-PSP	APSP	Cu-APSP	MPSP	Cu-MPSP	Range	Assignment
-	168	171	171		171	195-165	RCOO-RH (Standard oxidized cellulose) Carboxyl carbon of acetate group of hemicelluloses
-	-	164	164		164	169-140	C_6H_5O-RH Phenolic carbon
-	-	-	148		148	150-140	Subsituted oxygenated aromatic carbon
-	138, 129	130	138		131	135-120	Non oxygenated Aromatic carbons, Aromatic acids and anhydrides
100	101	101	112, 102	112, 101	101	102-108	Anomeric carbon (Anhydroglucose)C1
82	82	-		84, 79	85, 81	81-93	Anomeric carbon (Anhydroglucose)C4 amorphous cellulose~84
60, 70	70, 60, 52	62	61, 57	72, 61, 52	70, 61, 52	50-70	1^0 Alcohol of (Anhydroglucose) Aliphatic C-O C2,C3,C5(~70)C6(~60) amorphous cellulose~62
17	16	48, 36, 30, 18, 6	49, 36, 30, 16, 6	17	36, 30, 18, 8	5-50	Aliphatic C-C possibly of polymethylene type
SAPSP	Cu-SAPSP	PAPSP	Cu-PAPSP	9AAC	Cu-9AAC	Range	Assignment
170	-	171	167	-	192	195-165	RCOO-RH (Standard oxidized cellulose) Carboxyl carbon
-	-	163/146	146	-	-	169-140	C_6H_5O-RH Phenolic carbon
147	-	-	-	-	-	150-140	Subsituted aromatic carbon
-	122	130	138, 132	123	121	135-120	Aromatic carbons, Aromatic acids and anhydrides
111	-	101	116, 101	-	-	102-108	Anomeric carbon (Anhydroglucose)
-	-	-	-	-	-	81-93	Anomeric carbon (Anhydroglucose)
-	-	61, 55	61, 55	-	-	50-70	1^0 Alcohol of (Anhydroglucose) Aliphatic C-O
-	-	48, 35, 31, 16, 6	48,36, 30, 19, 14, 5	-	-	5-50	Aliphatic C-C

Cu-APSP and Cu- PSP showed a peak at 171ppm and 168 ppm respectively-similar to the-peak observed at 171 ppm in APSP and PAPSP which can be attributed to the carboxyl carbon (C-6), in the oxidized anhydroglucose unit of the cellulose chain formed after treatment with acid and persulfate respectively This peak is not seen in PSP and is of higher intensity in Cu-APSP than APSP indicating that adsorption of copper has caused changes in the c=o and c-o content as evidenced by XPS spectra. Similarly the peak at 93 ppm in Cu-APSP is attributed to C-1 of the terminal α-D-glucose unit that is usually present in oxidized cellulose .Moreover the peaks are seen to be sharper in Cu-PSP, APSP, Cu-APSP, PAPSP, Cu-PAPSP probably due to binding of Cu(II), and oxidation by acid and persulfate respectively which result in more ordered structures.

3.4. Mechanism.

In this work, several different modifications have been applied to improve/ modify the functional groups of palm shell powder and enhance the uptakes of metal ions. On the basis of FT-IR spectra as well as kinetic and isotherm modeling, the adsorption of Cd^{2+}, Zn^{2+}, Cu^{2+} and Hg^{2+} on the adsorbents could be considered to be via (1) Surface active functional groups like amine and carboxyl involving valence forces through the exchange of electrons, complexation, coordination and/or chelation and (2) Intraparticle diffusion into the micropores. The first step dominates at low concentrations while the latter step at high concentrations of Cd^{2+}, Zn^{2+}, Cu^{2+} and Hg^{2+}. These speculations are in agreement with the reported mechanisms [61-63].

Valeria et al. have reported that cadmium and zinc in aqueous solutions exist as Cd^{2+} and Zn^{2+} in solution till pH 8 and 7 respectively, beyond which the metal hydroxides starts precipitating in [64].

Hence, the probable mechanism by which M^{2+} are bound to carboxyl groups is:

$$2(-COOH) + M^{2+} \leftrightarrow (-COO)_2 - M + 2H^+$$

$$2(-COOH) + M(OH)_2 \leftrightarrow (-COO)_2 - M(OH) + H^+ + H_2O$$

$$(-COOH) + M(OH)^+ \leftrightarrow (-COO) - M(OH) + H^+$$

The binding mechanism of M^{2+} with phenolic groups could be:

$$2(-C_6H_5 - OH) + M^{2+} \leftrightarrow (-C_6H_5 - O)_2 - M + 2H^+$$

$$(-C_6H_5 - OH) + M(OH)^+ \leftrightarrow (-C_6H_5 - O) - M(OH) + H^+$$

A similar type of mechanism has been proposed for chromium adsorption onto agro-waste materials by Bernardo et al. [65]. Cd^{2+}, Zn^{2+}, Cu^{2+} and Hg^{2+}were considered to be

adsorbed due to binding with amino groups by electrostatic interaction as follows:

$$2(-NH_2) + M^{2+} \leftrightarrow (-NH)_2 - M + 2H^+$$

$$(-NH_2) + M^{2+} \leftrightarrow\equiv (-N - M) + 2H^+$$

$$(-NH_2) + M(OH)^+ \leftrightarrow (-NH) - M(OH) + H^+$$

$$(-NH_2) + M(OH)_2 \leftrightarrow (-NH)_2 - M(OH) + H^+ + H_2O$$

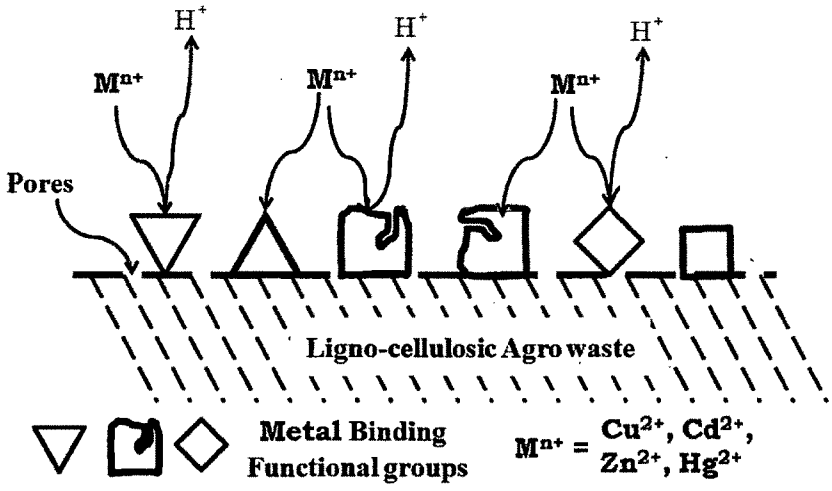

Scheme 3.1. Mechanism for binding of divalent metal ion

The XPS spectra confirmed the presence of Hg^0 and Hg^{2+} on the surface of PSP after mercury adsorption suggesting that reduction of Hg^{2+} to Hg^0 took place on PSP surface. This could be due to the oxidation of lignin aromatic carbons (aldehydic, phenolic and carboxyl groups) by Hg(II) and formation of alcoholic sites, carboxylic sites, CO_2 and elemental mercury.

$$Hg^{2+} + 2e^- \rightarrow Hg^0 \quad E^0 = +0.85\ V$$

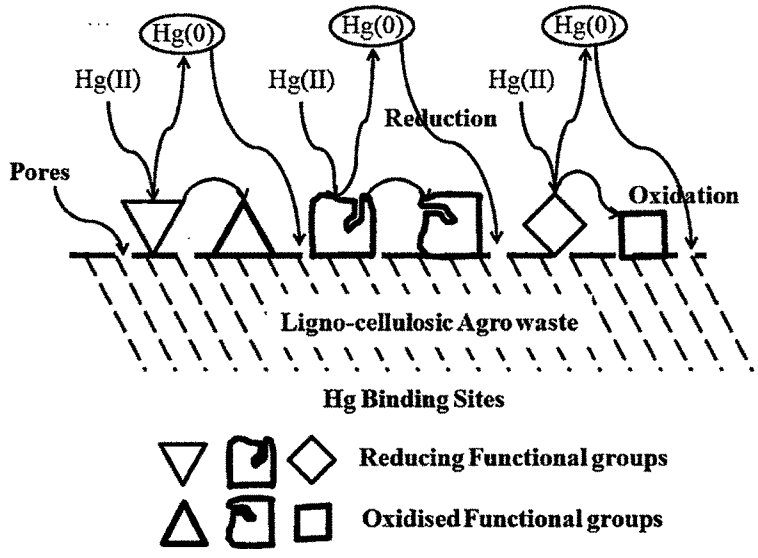

Scheme 3.2. Redox mechanism for mercury

E.I. El-Shafey reported reduction of Hg(II) to Hg(I) using sulfuric acid treated rice husk while M.Cox et al. reported reduction of Hg(II) to Hg(I) and Hg(0) using sulfuric acid treated flax shive [59, 60]. However there have been no literature reports on reduction of Hg(II) using virgin lignocellulosic materials though there have been reports on reduction of Cu(II) to Cu(0) and Cr(VI) to Cr(III) [57, 66]. Xin Huang et al have studied the adsorption of Hg(II) onto bayberry tannin-immobilised collagen fiber wherein they have reported the adsorption mechanism to be only chelation of Hg(II) [67]. Reduction of Hg(II) to Hg(0) has been reported on organic matter present in soil, fungi and other microorganisms [68-72].

3.5. Conclusions.

The prepared adsorbents show potential as effective systems for the removal of trace levels of metal ions from aqueous systems. Potentiometric, FT-IR and XPS studies reveal that carboxyl, amino, hydroxyl, lactonic and phenolic groups on PSP seem to be responsible for mercury adsorption. XPS studies showed different binding energies for Hg^{2+} and Cu^{2+} on the adsorbents under study indicating different types and degrees of chemical interaction of mercury and copper with surface functional groups. XPS studies also indicate that Hg(II) was reduced to Hg(0) on PSP surface and was adsorbed onto it by physisorption.

Sorption isotherms of the metal ions on the adsorbents were studied and modeled using Freundlich, Langmuir, Temkin, Dubinin-Radushkevich (DR), Elovich, Flory-Huggins, and Halsey isotherms. The adsorption data of the metal ions were best fit by Langmuir and Freundlich models.

Pseudo second order kinetics describes the overall sorption preocess well while intraparticle diffusion of the metal ion from the liquid phase to the adsorbent surface might be having some role up to variable extents in deciding the rate processes. The sorption process is exothermic, spontaneous and accompanied by decrease in entropy.

Adsorption of metals is thus a complex process that is based upon a range of mechanisms which differ according to the type of adsorbent, the degree of processing it has undergone and also the adsorbate. The different mechanisms which play a role include ion exchange, chelation and physisorption.In the case of mercury reduction of divalent mercury to elemental mercury also seems to play a role in the case of PSP.

The data obtained from column studies have shown good agreement with the predicted results obtained by application of Thomas model and Yoon and Nelson model as evident from the low value of standard deviation.

Adsorbent regeneration and metal recovery indicate the advantage of not producing any sludge. Thus based on the good uptake capacity, rapid kinetics, regenerability and low cost, the adsorbents under study prepared from palm shell appear to be promising for the removal of cadmium and zinc from aqueous solutions. Interestingly the adsorption capacity of 9AAC and PAPSP were found to be almost similar or sometimes lesser for 9AAC, thus proving that PAPSP is a more economical and efficient adsorbent as compared to 9AAC.

Literature Cited.

1. B. Volesky. *Trends Biotechnol* **1987**, *5*, 96.
2. L. Dambies, C. Guimon, S.Yiacoumi, E. Guibal. *Colloid Surf. A* **2001**, *17*, 203.
3. M.M. Figueira, B. Volesky, H.J. Mathieu. *Environ. Sci. Technol* **1999**, *33*, 1840.
4. E. Fourest, B. Volesky. *Environ. Sci. Technol.* **1996**, *30*, 277.
5. J. Buschmann, L. Sigg. *Environ. Sci. Technol.* **2004**, *38*, 4535.
6. S.F. Lim, Y.M. Zheng, S.W. Zou and J. Paul Chen. *Environ. Sci. Technol* **2008**, *42*, 2551.
7. B. Volesky, Z.R. Holen. *Biotech.Progress* **1995**, *11*, 235-250.
8. H. Biester, P. Schuhmacher, G. Muller. *Water Res.* **2000**, *34*, 2031.
9. Y.S. Ho. *Water Res.* **2006**, *40*, 119.
10. G. Bohart, E. Q. Adams. *J. Am. Chem. Soc.* **1920**, *42*, 523.
11. H. C. Thomas. *J. Am. Chem. Soc.* **1944**, *66*, 1664.
12. Y. H.Yoon, J. H. Nelson. *Am. Indian Hygiene Assoc. J.* **1984**, *45*, 509.
13. R. M. Clark. *EnViron. Sci. Technol.* **1987**, *21*, 573.
14. A. Wolborska. *Water Res.* **1989**, *23*, 85.
15. C. Hepplewhite, G. Newcombe, D.R.U. Knappe. *Water Sci. Technol.* **2004**, *49*, 257–265.
16. Langmuir. *J. Am. Chem. Soc.* **1916**, *38*, 2221–2295.
17. H.M.F. Freundlich. *Z. Phys. Chem.* **1906**, *57*, 385–470.
18. M.J. Temkin, V. Pyzhev. *Acta Physiochim* **1940**, *12*, 327.
19. P.J. Flory. *J. Chem. Phys* **1942**, *10*, 51.
20. M.L. Huggins. *Amt, N.Y. Acad, Sci* **1942**, *43*, 1.
21. P.J. Flory. *Discuss. Faraday Soc* **1970**, *49*, 7.
22. S.Y. Elovich, O.G. Larinov. *J. Physical Chemistry* **1962**, *2*, 209.
23. M.M. Dubinin, L.V. Radushkevich. *Proc Acad Sci USSR Phys Chem Sect* **1947**, *55*, 331.
24. G. Halsey. *J. Chem. Phys.* **1948**, *16*, 931.
25. S. Lagergren, K. Sven, *Vetenskapsakad Handlingar* **1898**, *24*, 1.
26. Y.S. Ho. Adsorption of heavy metals from waste streams by peat. Ph.D. thesis, University of Birmingham, Birmingham, UK, **1995.**
27. W.J. Weber Jr., J.C. Morris. *J. Sanitary Eng. Div. Proceed. Am. Soc. Civil Eng* **1963**, *89*, 31.
28. W.J. Weber, J.C.S. Morris, Proceedings of International Conference on Water Pollution Symposium. Oxford **1962**, *2*, 231.

29. W.J. Weber, J.C. Morris. Advances in water pollution research: removal of biologically resistant pollutants from waste waters by adsorption, in: International Conference on Water Pollution Symposium, Pergamon, Oxford **1962**, *2*, 231.
30. W. Rudzinsk, D.H. Everett. Adsorption of gases on heterogeneous surfaces. London: Academic Press; **1992**.
31. Y.S. Ho, G. McKay. *Ads Sci Technol* **2002**, *20*,797.
32. W. Rudzinski, T. Panczyk. *Adsorption* **2002**, *8*, 23.
33. G.E. Boyd, A.W. Adamson, L.S. Myers. *J. Am. Chem. Soc.* **1947**, *69*, 2836.
34. V.K. Gupta, I. Ali, Suhas, V.K. Saini, *J. Colloid Interface Sci* **2006**, *299*, 556.
35. P.X. Sheng, Y.P. Ting, J.P. Chen, L. Hong, *J. Colloid and Interface Sci* **2004**, *275*, 131.
36. D.K. Chattopadhyay, B. Sreedhar, V.S.N. Kothapalli, Raju. *Ind. Eng. Chem. Res.* **2005**, *44*, 1772-1779.
37. A. Seco, P. Marzal, C. Gabaldon , J. Ferrer. *J. Chem. Technol. Biotechnol* **1997**, *68*, 23.
38. T.K. Budinova, K.M. Gergova, N.V. Petrov, V.N. Minkova. *J. Chem. Technol. Biotechnol* **1994**, *60*, 177.
39. P. Marzal, A. Seco, C. Gabaldon, J. Ferrer. *J. Chem. Technol. Biotechnol* **1996**, *66*, 279.
40. J.P. Chen, L.Yang, *Ind. Eng. Chem. Res* **2005**, *44*, 9931.
41. S.B. Choi, Y.S. Yun. *J. Hazard. Mater* **2006**, *B138*, 378.
42. S.K. Das, A.R. Das, A.K. Guha. *Environ. Sci. Technol* **2007**, *41*, 8281.
43. K.V. Kumar, K. Porkodi. *J. Hazard. Mater* **2007**, *146*, 214.
44. R.E. Treybal. Mass Transfer Operations, third ed., McGraw-Hill, New York, **1980**.
45. G.S. ElShafei, I. N. Nasr, A.S.M. Hassan, S.G.M. Mohammad. *J. Hazard. Mater* **2009**, *172*, 1608.
46. J. Febrianto, A.N. Kosasih, J. Sunarso, Y.H. Ju, N. Indraswati, S. Ismadji. *J. Hazard. Mater* **2009**, *162*, 616.
47. G.J.L. Torresdey, K. Dokken, K.J. Tiemann, J.G. Parsons, J. Ramos, N.E. Pingitore, G. Gamez. *Microchem. J* **2002**, *71*, 157.
48. J.P. Chen. L. Yang. *Langmuir* **2006**, *22*, 8906.
49. V.K. Gupta, A. Rastogi. *J. Hazard. Mater* **2008**, *152*, 407.
50. K. Srividya, K. Mohanty. *Chem. Eng. J* **2009**, *155*, 666.

51. V.J. Inglezakis, S.J. Poulopoulos. Adsorption, ion exchange and catalysis: design of operations and environmental applications, By Elsevier **2006**, 339.
52. S.S. Baral, N. Das, T.S. Ramulu, S.K. Sahoo, S.N. Das, G.R. Chaudhury. *J. Hazard. Mater* **2009**, *161*, 1427.
53. L. Xiaomin, Y. Tang, C. Xiuju, L. Dandan, L. Fang, W. Shao. *Colloids and Surfaces A: Physicochem. Eng. Aspects* **2008**, *317*, 512.
54. F.R. Reinoso, A.L. Solano. Chemistry and Physics of Carbon, by Thrower, P. A.; Marcel Dekker, New York **1989**, *21*, 1.
55. X. Zeng, S. Prasad, S. Bruckenstein. *Langmuir* **1998**, *14*, 2535.
56. K.P. Lisha, S.M. Maliyekkal, T. Pradeep. *Chem. Eng. J* **2010**, *160*, 432.
57. L. Dupont, E. Guillon. *Environ. Sci. Technol* **2003**, *37*, 4235.
58. K.K. Krishnani, X. Meng, C. Christodoulatos, V.M. Boddu. *J. Hazard. Mater* **2008**, *153*, 1222.
59. E.I. El-Shafey. *J. Hazard. Mat* **2010**, *175*, 319.
60. M.Cox, E.I. El-Shafey, A.A.Pichugin, Q. Appleton. *J. Chem. Technol. Biotechnol* **1999**, *74*, 1019.
61. Y. Wang, X.W. Tang, Y.M. Chen, L.T. Zhan, Z.Z. Li and Q. Tang. *J. Hazard. Mater.* **2009**, *172*, 30.
62. Z. Li, X. Tang, Y. Chen, L. Wei, Y. Wang. *J. Hazard. Mater.* **2009**, *169*, 386.
63. Z. Li, T. Katsumi, S. Imaizumi, T. Xiaowu, T. Inui. *J. Hazard. Mater.* **2010**, *183*, 410.
64. M.N. Valeria, I. Villaescusa. *Coord. Chem. Rev.* **2008**, *252*, 1178.
65. G.R.R. Bernardo, R.M.J. Rene. *J. Hazard. Mater.* **2009**, *170*, 845.
66. J. G. Parsons, M. Hejazi, K. J. Tiemann, J. Henning, J. L.G. Torresdey. *Microchem. J.* **2002**, *71*, 211.
67. X. Huang, X. Liao, B. Shi. *J. Hazard. Mat* **2009**, *170*, 1141.
68. N. Belzile, G.J. Wu, Y.W. Chen, V.D. Appanna. *Science of the Total Environment* **2006**, *367*, 704.
69. B. Allard, I. Arsenie. *Water Air Soil Pollut* **1991**, *56*, 457.
70. C.L. Hansen, G. Zwolinski, D. Martin, J.W. Williams. *Biotechnol. Bioeng.* **1984**, *26*, 1330.
71. K. Schluter. *Environ. Geol.* **2000**, *39*, 249.
72. N.D. Hutson, B.C. Attwood, K.G. Scheckel. *Environ. Sci. Technol.* **2007**, *41*, 1747.